FINAL REPORT

07121-1603B. Final

Hydrate Plug Characterization & Dissociation Strategies
07121-1603b

September 1st, 2010

Principal Investigator
Dr. Michael Volk
Associate Vice President of Research & Technology Development
The University of Tulsa
800 South Tucker Drive
Tulsa, OK 74104

LEGAL NOTICE

This report was prepared by the University of Tulsa, as an account of work sponsored by the Research Partnership to Secure Energy for America, RPSEA. Neither RPSEA members of RPSEA, the National Energy Technology Laboratory, the U.S. Department of Energy, nor any person acting on behalf of any of the entities:

a. MAKES ANY WARRANTY OR REPRESENTATION, EXPRESS OR IMPLIED WITH RESPECT TO ACCURACY, COMPLETENESS, OR USEFULNESS OF THE INFORMATION CONTAINED IN THIS DOCUMENT, OR THAT THE USE OF ANY INFORMATION, APPARATUS, METHOD, OR PROCESS DISCLOSED IN THIS DOCUMENT MAY NOT INFRINGE PRIVATELY OWNED RIGHTS, OR

b. ASSUMES ANY LIABILITY WITH RESPECT TO THE USE OF, OR FOR ANY AND ALL DAMAGES RESULTING FROM THE USE OF, ANY INFORMATION, APPARATUS, METHOD, OR PROCESS DISCLOSED IN THIS DOCUMENT.

THIS IS A FINAL REPORT. THE DATA, CALCULATIONS, INFORMATION, CONCLUSIONS, AND/OR RECOMMENDATIONS REPORTED HEREIN ARE THE PROPERTY OF THE U.S. DEPARTMENT OF ENERGY.

REFERENCE TO TRADE NAMES OR SPECIFIC COMMERCIAL PRODUCTS, COMMODITIES, OR SERVICES IN THIS REPORT DOES NOT REPRESENT OR CONSTIITUTE AND ENDORSEMENT, RECOMMENDATION, OR FAVORING BY RPSEA OR ITS CONTRACTORS OF THE SPECIFIC COMMERCIAL PRODUCT, COMMODITY, OR SERVICE.

ABSTRACT

This report investigates the characteristics of hydrate plugs and the dissociation of those plugs. In order to study hydrate formation phenomena as well as hydrate dissociation rate and methods, 18 pumping and 19 low spot flow loop experiments were conducted.

In hydrate characterization studies, hydrate plugs were generated in the flow loop and characteristics such as density (ρ), porosity (φ) and permeability (k) were measured as a function of different operating parameters, such as different sub-cooling, salinity and gas injection rate. The operating parameters were varied to determine how hydrate formation time is affected. The porosities of the hydrates made in the low spot tests ranged from 0.7 to 0.86 and the permeabilities ranged from 2 *D* to 15 *D*.

Hydrate plugs made in low spot tests are found to be reproducible. Hydrate formation time depends on operating parameters such as gas injection, sub-cooling temperature and salinity. For the same operating parameters, the larger sub-cooling temperatures as well as the lower salinity formed hydrates faster and higher gas injection rate formed hydrate faster. It is hypothesized that these plugs would have become impermeable to gas if the gas flow was continued for a longer duration.

In hydrate dissociation studies, the hydrate plugs generated in the characterization studies were dissociated by different methods—heating, depressurization, and with glycol inhibitors. After analyzing the results from the dissociation

experiments, dissociation models were selected based on the results and different model simulations are compared.

Hydrates dissociated by heating dissociate uniformly along the length of the plug as models predict. In depressurization tests, the plugs did not appear to dissociate uniformly along the plug length. Inhibitors dissociate the plug when in contact. A first generation of inhibitor model was developed. Simulated dissociation with experimental temperature and pressure as inputs yields a better match between simulation results and experimental data than modeling without theses inputs.

Signature

4/18/11
Date

Michael Volk, Principal Investigator
University of Tulsa
Associate Vice President of Research and Technology Development

TABLE OF CONTENTS

Page

LEGAL NOTICE ii

ABSTRACT iii

SIGNATURE PAGE v

TABLE OF CONTENTS vii

LIST OF TABLES x

LIST OF FIGURES xi

CHAPTER 1: INTRODUCTION 1

CHAPTER 2: EXPERIMENTAL SETUP 4

2.1 Experimental Facility 4
2.1.1 Liquid Charge System 7
2.1.2 Gas Charge System 7
2.1.3 Seal Oil System 8
2.1.4 Cooling System 8
2.1.5 Boiler System 9
2.1.6 Instrumentation 9
2.2 Modifications and Test Procedure 10
2.2.1 Hydrate Formation Test Modifications 10
Pumping Tests 10
Low Spot Tests 11
2.2.2 Hydrate Formation Mechanism 12
2.2.3 Hydrate Dissociation Test Modifications 13
Pumping Tests 13
Low Spot Tests 14
2.2.4 Hydrate Formation Test Matrix 14
Pumping Tests 15
Low Spot Tests 15
2.3 Tested Fluids 16
2.3.1 Citgo 19 16
2.3.2 Natural Gas 17
2.3.3 Water/Brine 18

CHAPTER 3: EXPERIMENTAL RESULTS 19

3.1 Hydrate Characterization Studies 19
3.1.1 Hydrate Types 20
3.1.2 Pumping Tests 21
Permeability Calculations 22
Porosity Calculations 28
3.1.3 Low Spot Tests 29
Permeability Calculations 29
Scale-up 33
Hydrate Formation 33
Porosity Calculations 35
Flow Characteristic 36
3.2 Hydrate Dissociation Studies 39
3.2.1 CSM Model Selection 41
3.2.2 Dissociation Methods 43
Heating 45
Depressurization 45
Monoethylene Glycol 47
3.2.3 Comparison of Experimental Data with CSM Simulation 48
Mass Calculation 48
Heating 49
Depressurization 51
3.2.4 Comparison of TU Model and CSM-Plug Simulation 51
Heating 51
Overall Simulation Data Comparisons 53
3.2.5 Inhibitor Model 54

CHAPTER 4: CONCLUSIONS AND FUTURE WORK 57

4.1 Hydrate Characterization Conclusions 57
4.1.1 Pumping Tests 57
4.1.2 Low Spot Tests 58
4.2 Hydrate Dissociation Conclusions 59
4.2.1 Pumping Tests 60
4.2.2 Low Spot Tests 60
4.3 Future Work 61
4.3.1 Hydrate Characterization Studies 61
4.3.2 Hydrate Dissociation Studies 62

ACRONYMS 63

SYMBOLS 64

REFERENCES 65

APPENDIX A: 70

APPENDIX B: 72

APPENDIX C: 75

APPENDIX D: 77

APPENDIX E: 82

APPENDIX F: 86

LIST OF TABLES

Page

Table 2.1-1: List of Instrumentation 9

Table 2.2-1: Plug Experiments in Pumping Mode Test Matrix 15

Table 2.2-2: Low Spot Formation Experiments Test Matrix 16

Table 2.3-1: Citgo 19 Chemical Composition 17

Table 2.3-2: Tulsa City Gas Composition 18

Table 3.1-1: Permeability Data for Pumping Tests 22

Table 3.1-2: Low Spot Experiments Permeability Data 32

Table 3.1-3: Low Spot Experiments Porosity Data 36

Table 3.2-1: Dissociation Test Information 44

LIST OF FIGURES

Page

Figure 1.1-1: Hydrate Equilibrium Curve for Tulsa City Gas 1

Figure 2.1-1: Flow Assurance Loop Overview 5

Figure 2.1-2: Schematic of the Facility..... 6

Figure 2.2-1: Loop Configurations for Plug Generation in Pumping Mode 11

Figure 2.2-2: Loop Configurations for Low Spot Experiments 12

Figure 2.2-3: Low Spot Test Mechanism 13

Figure 2.2-4: Heating Dissociation Test Configuration 14

Figure 3.1-1: Moving Densitometer View and Density Trace 20

Figure 3.1-2: Hydrate Types Made in TU Flow Assurance Facility 21

Figure 3.1-3: Darcy's Law Scheme 23

Figure 3.1-4: Density Trace along the–HYD2008-025 24

Figure 3.1-5: Permeability Distribution along the Plug..... 24

Figure 3.1-6: Density Trace along the Pipe—HYD2009-014—Nonbridged 26

Figure 3.1-7: Non-bridged Case of Pumping Test during Measurement..... 26

Figure 3.1-8: Gas Channel Case of Pumping Test during Measurement 27

Figure 3.1-9: Hydrate Locations of Pumping Test during Measurement 28

Figure 3.1-10:Differential Pressure & Permeability—HYD2009-007 30

Figure 3.1-11:Differential Pressure & Permeability— HYD2009-005 31

Figure 3.1-12: Hypothesis—Plug Became Impermeable for Longer Gas Injection ……..32

Figure 3.1-13: Reproducibility of Hydrate Plugs–HYD2009-007 and 014..... 35

Figure 3.1-14: Flow Characteristic–HYD2009-007 and 008 38

Figure 3.1-15: Flow Characteristic—HYD2009-014 and 015 39

Figure 3.2-1: Hydrate Density Profile during Dissociation—HYD2008-017..... 40

Figure 3.2-2: Simulation Results for Pumping Experiments Using Two-sided Depressurization and Direct Heating 42

Figure 3.2-3: Density Traces of Heating Dissociation—HYD2009-015 45

Figure 3.2-4: Density Traces of Depressurization Dissociation—HYD2009-004 ... 46

Figure 3.2-5: Density Traces of Depressurization Dissociation—HYD2009-016 .. 47

Figure 3.2-6: Density Traces of MONOETHYLENE GLYCOL Dissociation — HYD2009-018..... 48

Figure 3.2-7: Density Integration—Experimental Mass 49

Figure 3.2-8: Simulation and Experimental Mass Change during Dissociation— HYD2009-015..... 50

Figure 3.2-9: Simulation and Experimental Mass Change during Dissociation— HYD2009-012..... 51

Figure 3.2-10: Simulation Comparison between *TU*'s Model and *CSM-Plug*— HYD2009-015 52

Figure 3.2-11: Simulation Comparison between *TU*'s Model and *CSM-Plug*— HYD2009-012..... 53

Figure 3.2-12: Dissociation simulations of Low Spot Experiments with *TU* Model and *CSM-Plug*..... 54

Figure 3.2-13: Scheme of Inhibitor Dissociation..... 55

A.1. Impermeable Hydrate Plugs-Bridged 70

A.2. Partial Hydrate Plugs 71

A.3. Deposits with Voids and Channels 71

B.1. Impermeable Hydrate Plugs-Bridged—HYD2008-014..... 72

B.2. Partial Hydrate Plugs— HYD2008-025..... 73

B.3. Deposits with Voids and Channels-Case 1— HYD2008-023 73

B.4. Deposits with Voids and Channels-Case 2— HYD2008-012 74

C.1. Pressure & Permeability Measurement of Impermeable Hydrate Plug under Gamma Scan..... 75

C.2. Huge Permeability Case due to Void Space..... 76

C.3. Uncertain Permeability due to Uncertain Length 76

D.1.1. Permeability Measurement—HYD2009-004 77

D.1.2. Permeability Measurement—HYD2009-005 78

D.1.3. Permeability Measurement—HYD2009-016 78

D.2.1. Permeability Measurement—HYD2009-007 79

D.2.2. Permeability Measurement—HYD2009-010 80

D.2.3. Permeability Measurement—HYD2009-014 80

D.2.4. Permeability Measurement —HYD2009-015 81

E.1. Model Simulation between *CSM-Plug* and *TU* Model—HYD2009-007..... 82

E.2. Model Simulation between *CSM-Plug* and *TU* Model—HYD2009-008..... 83

E.3. Model Simulation between *CSM-Plug* and *TU* Model—HYD2009-009..... 83

E.4. Model Simulation between *CSM-Plug* and *TU* Model—HYD2009-012..... 84

E.5. Model Simulation between *CSM-Plug* and *TU* Model—HYD2009-015..... 84

E.6. Model Simulation between *CSM-Plug* and *TU* Model—HYD2009-019..... 85

CHAPTER 1

INTRODUCTION

Hydrates are ice-like solid compounds which tend to form under high pressure and low temperature conditions when gas molecules are trapped into water.

The following Figure 1.1-1 is the hydrate equilibrium curve generated by *PVT-Sim* (version 18, 2008) based on the natural gas composition that we used to conduct hydrate formation tests.

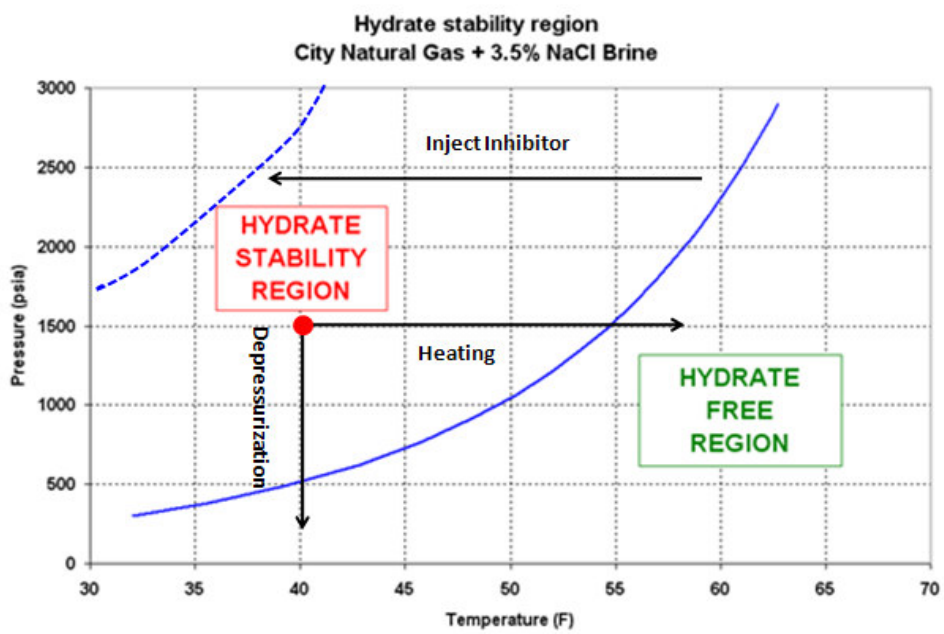

Figure 1.1-1: Hydrate Equilibrium Curve for Tulsa City Gas

This figure shows that under high pressure and low temperature conditions, hydrates are formed and tend to be stable. On shut-in, the line temperature cools very

rapidly to that of the ocean floor (40°*F* for depths greater than 3000 *ft*) so that the system is almost always in the hydrate region if the line is not depressurized. At that condition, multiple hydrate plugs can form. An understanding of how hydrates form deposits and how this leads to hydrate plug formation in subsea satellite wells, flow-lines and risers is important to avoid plugging in deepwater production operations. When thermodynamic inhibitors such as salt, glycol or methane are added to the system, the hydrate equilibrium curve moves to the left (i.e., it moves to lower temperature and higher pressure side.) This inhibits hydrate formation. But sometimes the flow-lines are not well inhibited, and thus hydrates form. In this case, the hydrate plug must be dissociated before production can resume. Based on this figure, dissociation will occur if the temperature increases, the pressure decreases, or inhibitors are added.

The main objective of this investigation is to prevent hydrate formation and provide guidelines for hydrate dissociations in the real operating environment by understanding hydrate formation phenomena and dissociation methods and efficiencies.

In order to fulfill the purpose of scientific research investigations, the author conducted this work with the three fundamentals of the scientific method. First, enough experimental data were acquired through data acquisition system and visual observations to suggest a problem. Second, the information was examined to ensure an isolation of false interpretations and point of views, allowing classification as evidence. Third, based on the deductive knowledge and relationship between evidence and literature, groups of hypotheses are drawn as follows:

1. Hydrate formation time depends on operating parameters such as gas injection, sub-cooling temperature and salinity. For the same operating parameters, the

larger sub-cooling temperatures formed hydrates faster while higher gas injection rates formed the hydrate plugs faster. Also higher salinity delayed the hydrate formation.

2. When heating was used to dissociate hydrate plugs, the plugs dissociated uniformly.
3. Inhibitors dissociate the plug where they are in contact.

As the above ideas are only hypotheses, they are not provided as absolute truth. However, they are the beginning for experimental reasoning as observed during analysis of experiments in Chapter 3.

This study can be categorized as an experimental investigation where the design of the experiments presented in Chapter 2 is very important.

Chapter 3 describes hydrate plugs made for 18 pumping tests and 16 low spot tests that simulate a leaky valve scenario. The plugs were characterized by calculating permeability, porosity and flow characteristic. The 18 pumping tests were all dissociated by heating. During the 16 low spot tests, 11 of them were dissociated by heating, 4 of them were dissociated by depressurization and 1 dissociated by Monoethylene Glycol (MEG). Chapter 3 discusses the test analysis as well as the validity of the previous hypotheses established. Furthermore, the dissociation experimental data are compared with model simulations.

Chapter 4 summarizes the conclusions of this investigation both on characterization and dissociation. Future work is proposed as well.

CHAPTER 2

EXPERIMENTAL SETUP

2.1 Experimental Facility

The experiments were conducted in the University of Tulsa Hydrate flow loop which consists of 160 *ft* of Schedule 80 stainless steel pipe with the inside diameter of 2.9 inches. This flow loop has been used for the research of plugging tendencies of hydrate forming systems during restart operations for Douglas Estanga's Master (2007) thesis and hydrate formation experiments for Colorado School of Mine's Hydrate Research Center (2008) as well. The flow loop is connected at both ends to the suction and discharge sides of a multiphase pump. The pipe forms a closed flow path in which fluids may be introduced and is jacketed with a 5 inch Schedule 10 stainless steel pipe over most of its length except around the multiphase pump. Four gamma ray densitometers are installed on the pipe, three of which are fixed and one that scans a 39 *ft* length. The fixed ones give the density trace at certain point and plot the density profile as a function of time. The moving densitometer plots the density trace along the scanning distance which is 39 *ft* long. All the equipment necessary to charge oil, water, gas and additives into the flow loop is stored at the process building which is at the left side of the flow loop in Figure 2.1-1. The control trailer, which faces the flow loop, contains all the data acquisition modules and the operator computer interface. A boiler system has been added to the original facility as well as a boiler room.

Figure 2.1-1: Flow Assurance Loop Overview

A detailed schematic view of the flow loop is shown in Figure 2.1-2. The entire flow loop is mounted on an 80 *ft* long deck that can be rocked back and forth with maximum amplitude of +/- 8 degrees and a minimum period of 30 seconds to set the fluid in motion using a rocking mode. The fluids can be pumped with the Leistritz twin-screw multiphase pump from horizontal up to 8 degrees uphill (the pump does not operate with a downhill discharge to prevent it from running dry). The maximum flow rate displaced by the pump is about 250 *GPM*, which corresponds to a 12 *ft/s* maximum fluid velocity. The pump suction and discharge pressures are measured as well as the pressure drop across each leg and the overall pressure drop. Several temperature probes are mounted on the outside pipe wall of the inner pipe and the inside pipe wall of the inner pipe.

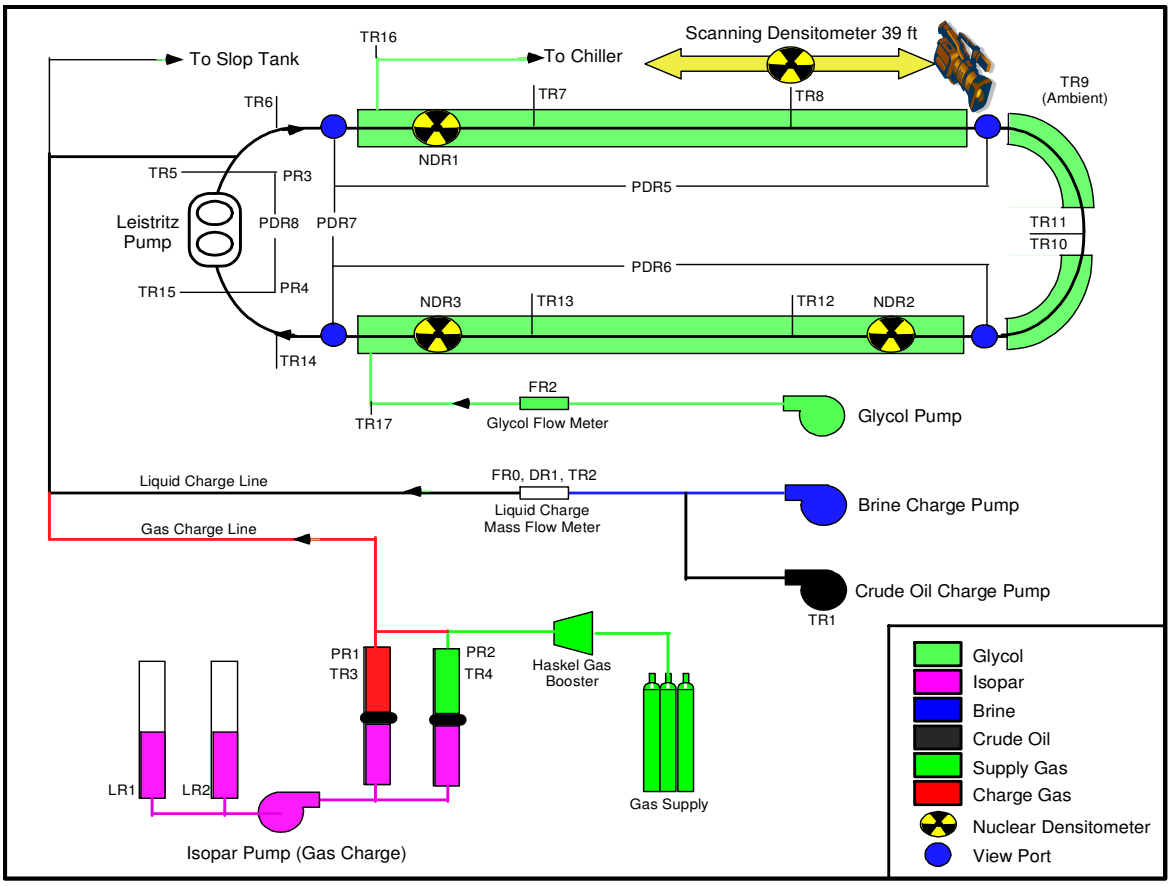

Figure 2.1-2 Schematic of the Facility

Glycol is used as a coolant in the annulus and can be set to flow co-current or counter-current with respect to the process fluids. Inlet and outlet temperatures of the coolant are measured and the average glycol temperature is used to control cooling ramps. A 20 *ton* chiller is used to cool the glycol. The glycol flow rate is also measured and is maintained constant during each test. Four view ports at the beginning and end of each leg are used to observe the hydrate formation. These view ports are made up of three sapphire windows at 120 degrees from each other around the pipe. Video systems allow us to record videos of the hydrate formations and dissociations. Three fixed gamma densitometers are also used to collect density data of the process fluids to quantify the density profile as a function of formation time. One moving gamma densitometer is used

to collect density data and provide the density profile as a function of scanning distance (39 *ft*) during the experiment.

2.1.1 Liquid Charge System

Brine, oil, solvents and additives can be charged from the equipment in the process building. Typically, oil, brine and solvents are charged into the flow loop at low pressure using gear pumps. The amount of each phase loaded in the flow loop is measured by a Micro Motion mass flow meter and recorded by the computer system. Water and additives can also be injected at a very slow rate while the facility is pressurized using a Milton-Roy high pressure piston pump. A brine preparation system is used to prepare brines from tap water prior to injection into the flow loop. Crude oil is circulated and heated prior to injection into the flow loop to ensure dissolution of any precipitated material such as paraffin. The charge lines are heat-traced and insulated to prevent freezing, gelling and/or wax deposition.

2.1.2 Gas Charge System

Gas is introduced into the flow loop by volumetric displacement using high-pressure cylinders and a high-pressure piston pump. Two cylinders are used alternatively, one being charged from the gas supply while the second is being transferred into the flow loop. Pressure and temperature of the gas leaving the cylinder are measured as well as the displaced volume of Isopar oil; the mass of gas introduced into the flow loop is then computed using equations of state and input compositions. The system allows use of the Peng-Robinson (PR), Redlich-Kwong (RK) or Benedict-Webb-Rubin (BWR) equations

of state in the gas mass computation. The gas addition system can be set to charge a given mass of gas into the system and/or maintain a set pressure in the flow loop. For constant pressure tests, the measured amount of gas injected into the facility is a measurement of the hydrate formation. This system is called "gas system" later in this thesis. Gas system gives a 0.2 *lb/min* maximum gas injection rate to the flow loop. The cycle between the cylinder change is around every 10 minutes. In 2008, a compressed natural gas (CNG) system was connected directly to the flow loop. This system is called "CNG" system later in the report. The CNG system gives a higher gas flow rate of 2 *lb/min* while maintaining a constant temperature for permeability measurements; however the gas charged from the "CNG" system pulsed approximating every 45 minutes. The gas flow in for this injection system is measured using micro motion meter.

2.1.3 Seal Oil System

A John Crane seal oil system is used to maintain back-pressure on the multiphase pump seals as well as provide cooling and lubrication. This seal system constantly adjusts the back-pressure on the seals to track the flow loop pressure. An accumulator also keeps the pressure on the seals in case of a power failure, allowing sufficient time for the operators to depressurize the flow loop and bring the system to a safe condition.

2.1.4 Cooling System

A 20 *ton* chiller is used to cool the glycol that circulates in the annulus. The glycol is also used to cool the seal oil and the video equipment. Temperature ramps can be programmed up to about 40 °*F/hr*. The glycol is circulated using a centrifugal pump

and the glycol flow rate is measured with a magnetic flow meter. A second holding tank equipped with steam coils and another centrifugal pump is used to hold and circulate glycol at temperatures higher than 85°*F*. A shell-and-tube steam heat exchanger is also used to heat the glycol circulating in the annulus during the hydrate dissociation phase.

2.1.5 Boiler System

Steam is required as a heat source in this facility for controlling the flow loop temperature, especially during the hydrate dissociation phase, as well as providing heat tracing for the liquid charge lines and avoiding plugging or freezing during winter conditions. A 450,000 *Btu/hr* boiler was installed in a boiler room. The boiler room also hosts a 25 *HP* air compressor to actuate the control valves, sump pump and gas booster.

2.1.6 Instrumentation

The flow loop is instrumented mainly with Rosemont pressure and differential pressure transducers and temperature transducers (RTDs). A Micro Motion Coriolis flow meter records the amounts of liquids charged into the flow loop. Table 2.1-1 provides a list of the principal instruments on the facility.

Table 2.1-1: List of Instrumentation

Name	Description	Range		Unit
		Min	Max	
AI1	Loop Inclination Angle	-166.6	166.6	*Degree*
DR1	Micro Motion Density	0	1.2	*g/cc*
FR2	Glycol Flow Meter (Fisher)	0	583.3	*GPM*
LR1	Isopar Tank A Level (DP)	0	33.3	*inch* H_2O
LR2	Isopar Tank B Level (DP)	0	33.3	*inch* H_2O
NDR1	Nuclear Density Gauge #1	0	1.2	*g/cc*

Name	Description	Range		Unit
		Min	Max	
NDR2	Nuclear Density Gauge #2	0	1.2	*g/cc*
NDR3	Nuclear Density Gauge #3	0	1.2	*g/cc*
PDR4	John Crane Seal Differential Pressure	0	200	*psi*
PDR5	Loop Differential Pressure East	0	36	*psi*
PDR6	Loop Differential Pressure West	0	36	*psi*
PDR7	Loop Differential Pressure	0	36	*psi*
PDR8	Leistritz Differential Pressure	0	36	*psi*
PR1	Piston Vessel A Gas Pressure	0	3000	*psi*
PR2	Piston Vessel B Gas Pressure	0	3000	*psi*
PR3	Loop Inlet Pressure (Leistritz Discharge)	0	2500	*psi*
PR4	Loop Outlet Pressure (Leistritz Suction)	0	2500	*psi*
PR5	John Crane Seal Pump Pressure	0	2500	*psi*
TR02	Micro Motion Temperature	-50	250	*°F*
TR03	Piston Vessel A Temperature	0	200	*°F*
TR04	Piston Vessel B Temperature	0	200	*°F*
TR05	Loop Temperature @ 1.3-ft from Pump Discharge	0	200	*°F*
TR06	Loop Temperature @ 6.3-ft from Pump Discharge	0	200	*°F*
TR07	Loop Temperature @ 27.1-ft from Pump Discharge	0	200	*°F*
TR08	Loop Temperature @ 51.9- ft from Pump Discharge	0	200	*°F*
TR09	Ambient Temperature	0	200	*°F*
TR10	Loop Temperature @ 80.5-ft from Pump Discharge	0	200	*°F*
TR11	Loop Temperature @ 88.3-ft from Pump Discharge	0	200	*°F*
TR12	Loop Temperature @ 109.1-ft from Pump Discharge	0	200	*°F*
TR13	Loop Temperature @ 133.7-ft from Pump Discharge	0	200	*°F*
TR14	Loop Temperature @ 154.9-ft from Pump Discharge	0	200	*°F*
TR15	Loop Temperature @ 159.7-ft from Pump Discharge	0	200	*°F*
TR16	East Jacket Glycol Temperature	0	200	*°F*
TR17	West Jacket Glycol Temperature	0	200	*°F*
TR18	Seal Oil Temperature South	0	200	*°F*
TR19	Seal Oil Temperature North	0	200	*°F*

2.2 Modifications and Test Procedure

Hydrates can be formed in the flow loop while pumping or in a low spot configuration; however, several modifications were required to accomplish this. These changes are discussed below.

2.2.1 Hydrate Formation Test Modifications:

Pumping Tests:

In order to better conduct hydrate formation pumping tests, the following modifications to the existing flow loop facility were made and shown in Figure 3.2-1.

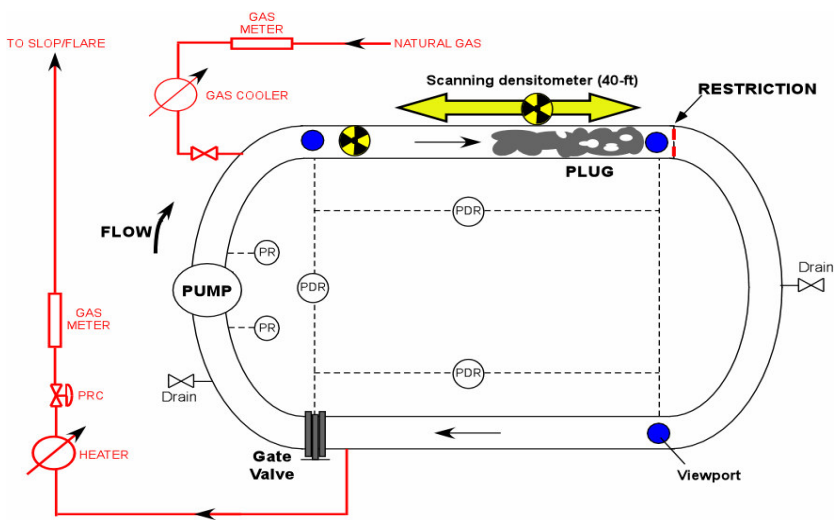

Figure 2.2-1: Loop Configurations for Plug Generation in Pumping Mode

- A flow restriction piece was inserted through a viewing window because it was hypothesized that it would help create the plug under the scanning gamma densitometer. The restriction plate is 2.8 inches long and 1 inch wide.
- The CNG system was installed allowing a higher gas circulation rate around 2 *lb/min* while maintaining a constant temperature for permeability measurements.

- Valves and ports were installed to drain the free liquids after the plug was formed and to collect the plug-trapped fluids released during permeability measurements.

Low Spot Tests:

In order to simulate a leaky valve scenario, the pump was not using during the entire experiment. Gas was bubbled into the flow loop instead of circulating the fluid by multiphase pump, as shown in Figure 2.2-2.

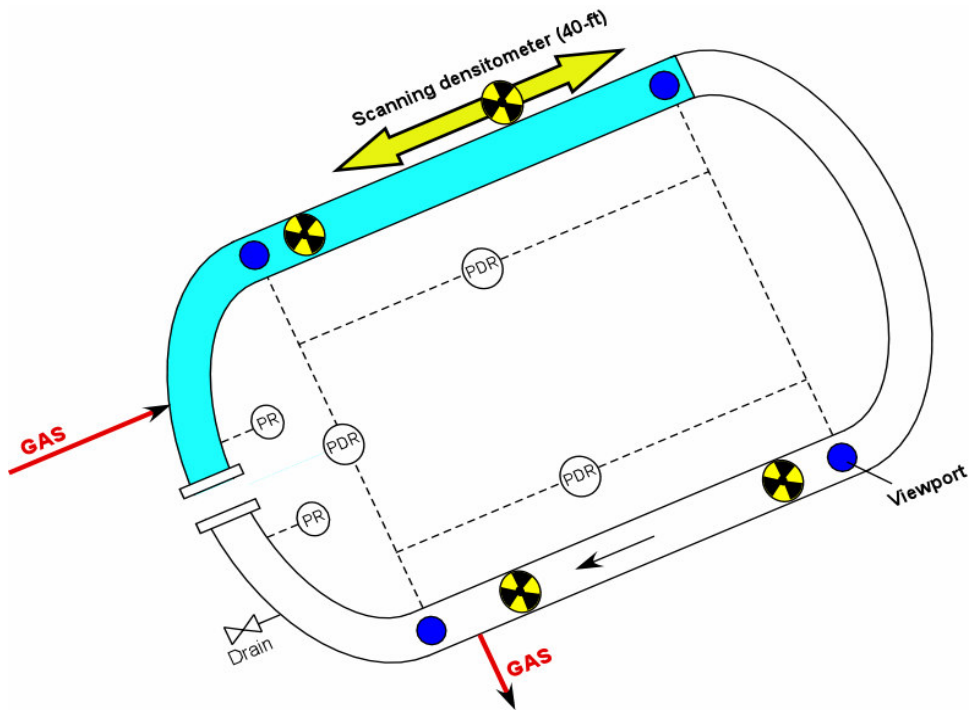

Figure 2.2-2: Loop Configurations for Low Spot Experiments

2.2.2 Hydrate Formation Mechanism:

In this low spot test configuration, the pump was taken out and one leg was charged with water under hydrate-forming conditions. The hydrate formation procedure is divided into four steps as shown in Figure 2.2-3. The first step in the experiment is to charge water into one leg of the pipe with the jacketed glycol temperature at 70 ^{o}F and

then pressurize the loop to the required pressure (in most cases 1500 *psi*). Then, the system is cooled to form the hydrate plug (in most cases 40 ^{o}F). The second step is the "gas restart" step. In a hydrate-stable condition, gas is bubbled at the lower end of the pipe with a low gas injection rate of 0.2 to 2 *lb/min*. Step 3 is the hydrate forming step—as the gas encounters water under the correct pressure and temperature, hydrates accumulate in the pipe and water is slowly displaced by the hydrates. At step 4, the entire pipe is filled with hydrates and after the system has stabilized, the whole hydrate formation is done. Gas is then injected through the hydrate plug while measuring the pressure drop. This data is then used to calculate the permeability of the plug using *Darcy's law*.

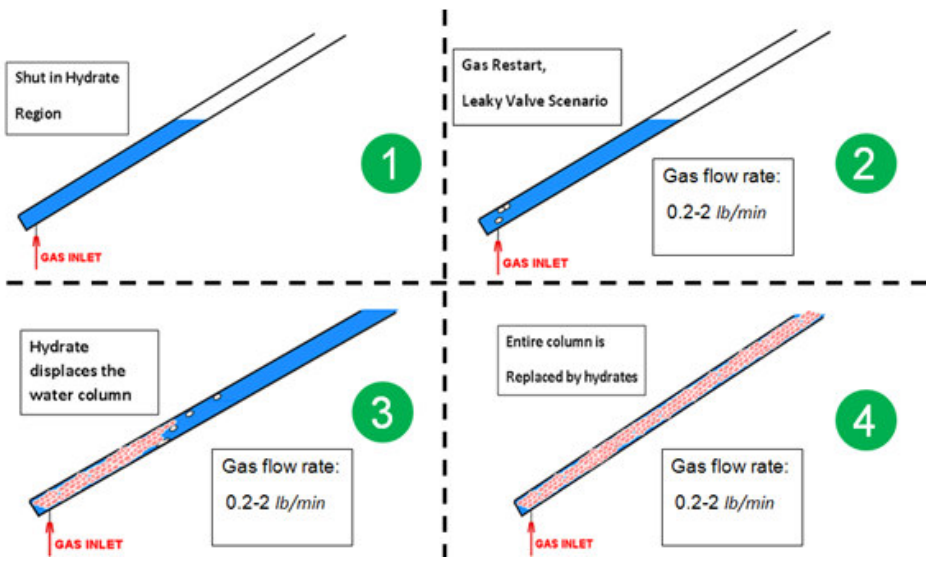

Figure 2.2-3: Low Spot Test Mechanism

3.2.3 Hydrate Dissociation Test Modifications:

Pumping Tests:

For the pumping tests, hydrate characterization is the main study objective, so the dissociation was achieved quickly (less than 4 hours) by heating up the glycol and

creating a large driving force during dissociation. In the following low spot tests, dissociation procedures were developed for the dissociation studies.

Low Spot Tests:

After all the data of the low spot tests were processed, a dissociation procedure was developed to dissociate hydrates. An inclination angle of +/-2 degree was needed to allow the water to drain and yet prevent the plug from collapsing when first starting to dissociate. Density traces were taken every 10 to 15 minutes to get the mass change. After a step in temperature (heating) or pressure (depressurization), another step was not taken until integration of the gamma scan mass stabilized. Water was drained when observed at the lower view port to prevent the water accumulation under the density scan. One example of heating dissociation is shown in Figure 2.2-4.

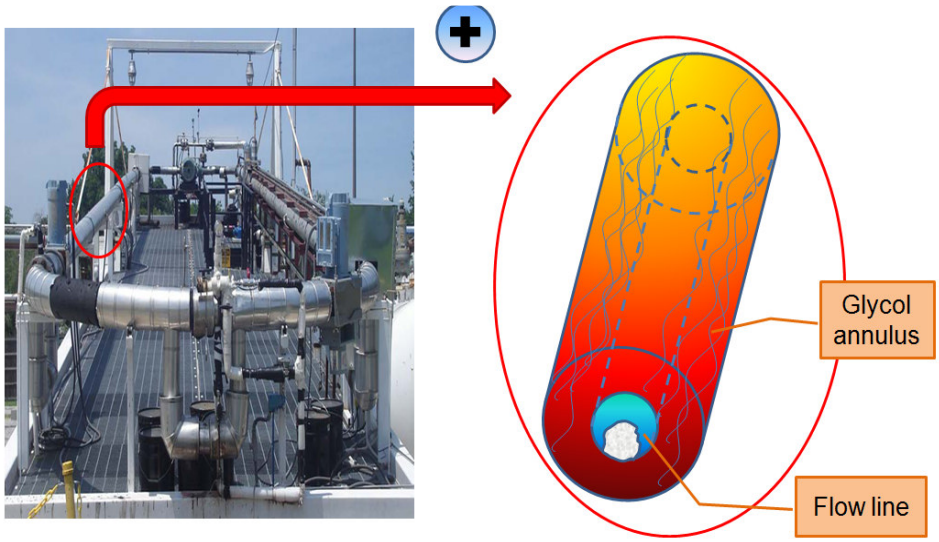

Figure 2.2-4: Heating Dissociation Test Configuration

2.2.3 Hydrate Formation Test Matrix:

Of all the hydrate formation tests, 18 tests were conducted under pumping mode and 16 tests were conducted under low spot mode. Test matrices are listed in Table 2.2-1 and Table 2.2-2 respectively.

Pumping Tests:

18 hydrate formation tests under pumping mode were conducted in which the water cut of these tests ranged from 25% to 65% in volume and liquid loading ranges from 50% to 75 % in volume. Salinity varies from 0 % to 7 % based on weight. The detailed test matrix is listed in Table 2.2-1.

Table 2.2-1: Plug Experiments in Pumping Mode Test Matrix

Test #	Liquid Loading (% Volume)	Water Cut (% Volume)	Salinity (% wt.)	Notes
HYD2008-011	50	50	0	Gas Channel
HYD2008-012		25		No Plug
HYD2008-013		37.5		No Plug
HYD2008-014	75	50		Impermeable in Pipe
HYD2008-015	50			No Plug
HYD2008-016			3.5	Unknown Length
HYD2008-017	75	50	3.5	Gas Channel
HYD2008-018				Gas Channel
HYD2008-019				No Plug
HYD2008-020				Gas Channel
HYD2008-021	75	37.5	0	No Plug
HYD2008-022		50	3.5	Gas Channel
HYD2008-023			7	Unknown Length
HYD2008-024	75	50	3.5	No Plug
HYD2008-025				Impermeable in U or other
HYD2008-026				Gas Channel
HYD2008-028		65		No Plug
HYD2008-028		50		No Plug

Low Spot Tests:

16 hydrate formation tests using low spot mode were conducted with 100% water cut. Gas injection rates were 0.2 *lb/min* and 2 *lb/min*. Salinity ranged from 0 to 14%. Sub-cooling temperature ranged from 5 °*F* to 21 °*F*. The detailed test matrix is listed in Table 2.2-2.

Table 2.2-2: Low Spot Formation Experiments Test Matrix

Test #	Gas Injection Rate lb/min	Salinity %	Sub Cooling F
HYD2009-013	0.2	0	5
HYD2009-012			10
HYD2009-003			21
HYD2009-011		14	7
HYD2009-010		7	15
HYD2009-009			
HYD2009-015		3.5	10
HYD2009-014			11
HYD2009-008			18
HYD2009-007			
HYD2009-006			
HYD2009-019	2		
HYD2009-018			
HYD2009-016			
HYD2009-005			
HYD2009-004		0	21

2.3 Tested Fluids

In the pumping tests, Citgo 19, natural gas and water were selected to form hydrate in order to simulate a production environment. In the low spot tests, in order to simulate a leaky valve scenario, water with different salinities and natural gas were selected to conduct the formation tests.

2.3.1 Citgo 19

For the pumping tests, Citgo 19 was selected as the oil phase to form hydrates. It is a non-adhesive mineral oil mainly used for lubrication purposes, which is a good

choice to record visual observation during the experiments due to its bright clear appearance. As its API gravity is only 32.9°, it is categorized as light oil. The density of Citgo 19 is 860 kg/m^3 under standard conditions. Table 2.3-1 shows the chemical composition of this oil in terms of weight percentage.

Table 2.3-1: Citgo 19 Chemical Composition

Component	Weight [%]
C14	0
C15	0.01
C16	0.01
C17	0.05
C18	0.19
C19	0.64
C20	1.72
C21	2.72
C22	7.27
C23	12.30
C24	14.33
C25	13.63
C26	11.87
C27	11.36
C28	8.93

Component	Weight [%]
C29	5.67
C30	3.36
C31	1.78
C32	1.26
C33	0.71
C34	0.59
C35	0.42
C36	0.29
C37	0.27
C38	0.20
C39	0.21
C40	0.13
C41	0.08
Total	100

2.3.2 Natural Gas

Tulsa City gas was used for the gas charge. The density of the gas at test conditions of 1500 *psi* and 40 °*F* is 96 kg/m^3. Table 2.3-2 shows the chemical composition of Tulsa City gas in terms of molecular percentage.

Table 2.3-2: Tulsa City Gas Composition

Component	Mole [%]
N_2	1.05
CO_2	1.23
C1	94.91
C2	2.35
C3	0.38
iC4	0.02
nC4	0.06
Total	100

2.3.2 Water/Brine

Fresh tap water and brines with salinities of 3.5%, 7% and 14% were selected as the aqueous phase. The brine solutions were prepared by dissolving 99.99% sodium chloride tablets to fresh tap water.

CHAPTER 3

EXPERIMENTAL RESULTS

The following section provides detailed test information on both hydrate characterization and dissociation studies during this investigation. Analyses are mainly based on the density traces, pressure measurements, temperature measurement, pressure drop and visual observations as well as simulation comparisons. As this investigation is about both hydrate characterization and dissociation studies, results are divided into two parts. The hydrate plug formation and characterization study are discussed first. Different hydrate plug types were made by varying salinity, sub-cooling temperature and gas injection rate. The discussion is followed by the hydrate plug dissociation study. Models were selected based on the experimental data and the simulation results were compared with experimental data.

3.1 Hydrate Characterization Studies

The experimental results of the hydrate characterization study will be fully discussed in this section. In order to study the hydrate plug types, how permeability and formation time are affected by different operation parameters. Two sets of experiments were conducted; pumping tests and low spot tests were used. For both the pumping and

low spot tests, the moving gamma densitometer was used to measure the hydrate plug densities along the scanning distance. They provide very important information for hydrate permeability calculations and as well as the calculation of mass of hydrate remaining in the pipe. Density inside the pipe was recorded every half inch, i.e., 925 points of density are recorded on a distance of 39 *ft* to generate a density trace. Figure 3.1-1 shows a picture of the gamma densitometer and an example density trace after hydrates formed.

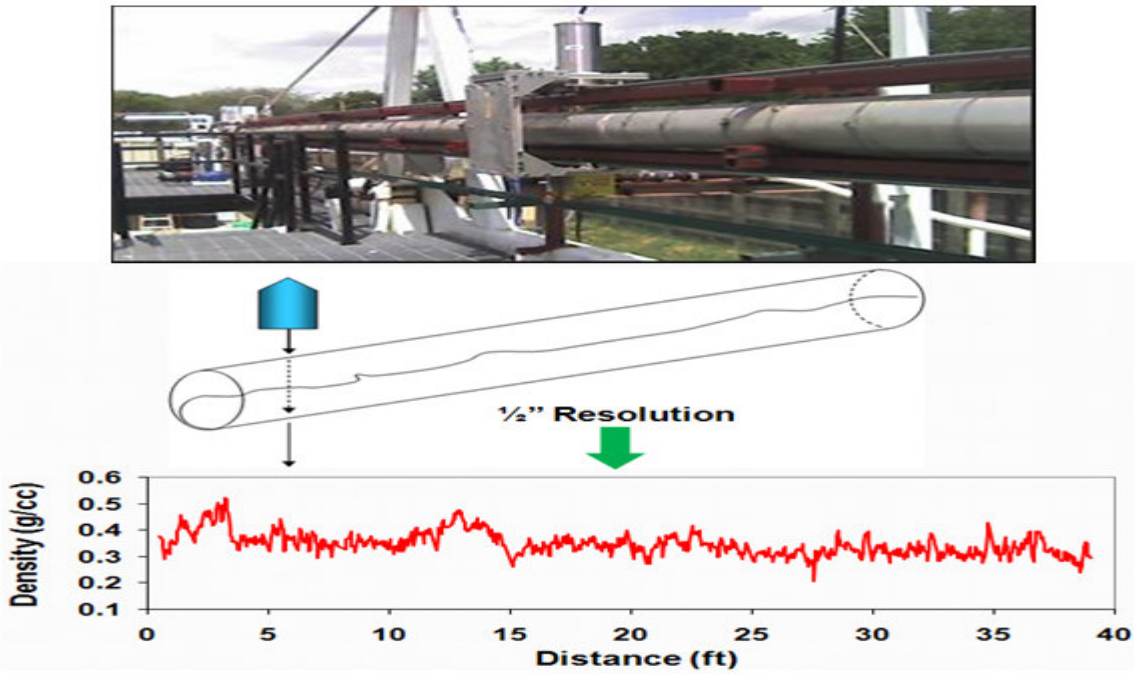

Figure 3.1-1: Moving Densitometer View and Density Trace

3.1.1Hydrate Types

We have categorized hydrates in as slurry, porous or dense, which have the consistencies of margarita slurries, a pile of glass beads and compacted snow respectively. The slurry type hydrates made by the TU flow loop are similar to the slurry like or slush like ones made by Fang-and Wang (2008). The porous type hydrates are not

similar to any of the hydrate in the literature. Figure 4.1-2 presents pictures of hydrates made in our test loop.

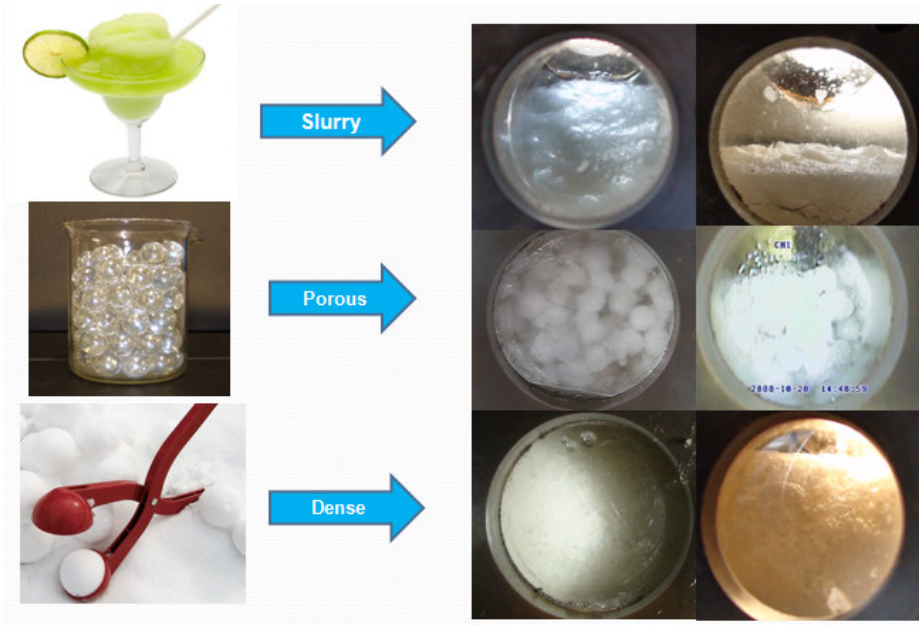

Figure 3.1-2: Hydrate Types Made in TU Flow Assurance Facility

3.1.2 Pumping Tests

In the 18 pumping tests, hydrate plugs did not form where the blocking plate was located as hypothesized. Some plugs formed after the blocking plate or in the U-section. Plugs generated in the pumping mode did not form by agglomeration as hypothesized; what we formed in most of the experiments were hydrate slurries. These experiments were run at liquid loadings ranged from 50% to 75% by volume and water cut ranged from 25% to 65% by volume. For these experiments, no water was recovered indicating that most of the water remained trapped in the hydrate or was converted to hydrate. For the tests where plugs were formed, permeabilites were calculated and are noted in Table 3.1-1.

Table 3.1-1: Permeability Data for Pumping Tests

Test #	Permeability (D)		Plug Length (ft)		Notes
	Pipe	U Section	Pipe	U Section	
HYD2008-011	45-65	---	20	---	Gas channel
HYD2008-014	0	---	fully bridged	---	PDR 5 hold 158 psi for 1 hr and no gas out
HYD2008-016	6-8	24-29	2	16	2 ft from gamma scan
HYD2008-017	18-55	---	5-15	---	Gas channel
HYD2008-018	10-17	---	39-65	---	Gas channel
HYD2008-020	25-42	---	39-65	---	Gas channel
HYD2008-022	8-16	2-4	28-53	16	Gas channel
HYD2008-023	3	---	5	---	3 ft from gamma scan
HYD2008-024	---	0	---	---	PDR6 hold 80 psi for 0.75hr and no gas out
HYD2008-026	10-60	---	15	---	10 D measured by gas system and 60 D when higher gas flow rate used

In the above table, the first column indicates the test number. The second column indicates the permeability calculated from *Darcy's law*. The first sub column represents the permeability calculated assuming that hydrate plugs were formed under the gamma scanning zone and the second sub column represents the permeability calculated assuming that hydrate plug was formed in the *U* or the other leg. The third column indicates the hydrate plug length used during the permeability calculation while the first sub column represents the length under the gamma scanning zone and the second sub column represents the length in the *U* or other leg. All the lengths used under the gamma scanning zone were extracted from density traces. The fourth column shows all the notes. In the tests which are not shown, hydrate deposits did form in the flow loop, but they did not form plugs that blocked the loop.

Permeability Calculations:

After a plug was formed, pressure drop measurements were made to calculate permeability. Gas was circulated through the plug; differential pressure and gas flow rate

were measured. Permeability was calculated according to *Darcy's law*, shown in Figure 3.1-3, Equation 3-1.

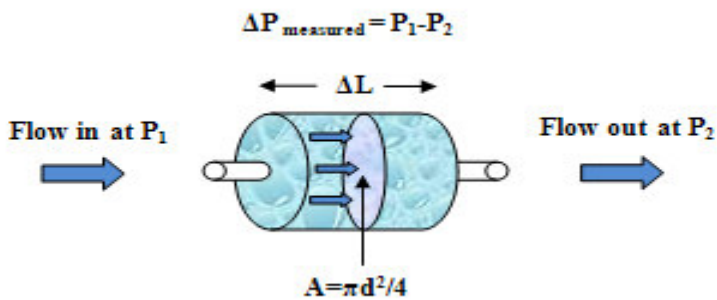

Figure 3.1-3 Darcy's Law Scheme

$$q = \frac{k\,A}{\mu}\frac{\Delta p}{\Delta l} \Rightarrow k = \frac{v\,\mu \Delta l}{\Delta p} \quad (3-1)$$

Uncertainties in the permeability measurement for the pumping tests were due to the following reasons:

1. Variable permeability/density along the plug
2. Whether the hydrate deposit plugged (bridged) or not
3. Whether there was a gas channel through or on top of the plug
4. Unknown length/location of the plug

Case 1: Variable Permeability:

Figure 3.1-4 is an example of density traces before and after draining water during hydrate formation time.

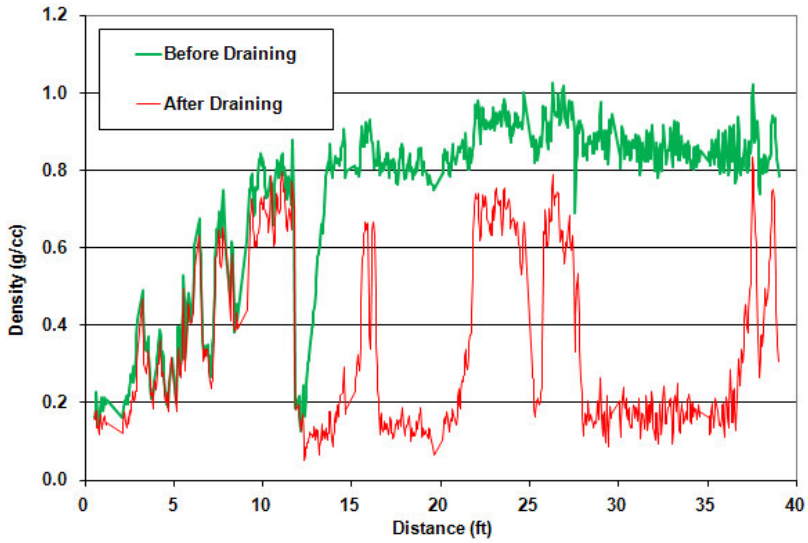

Figure 3.1-4: Density Trace along the Pipe for HYD2008-025—Nonuniform

In this figure, the vertical axis represents the hydrate density in *g/cc* and horizontal axis represents the scanning distance by *ft*. The green trace shows the density trace before draining and red one shows the density trace after draining. After draining, the highest density inside the pipe is around 0.8 *g/cc* and the lowest density inside the pipe is around 0.15 *g/cc*. 0.8 *g/cc* density indicates the pipe is pretty much filled with hydrate and 0.15 *g/cc* indicates that the pipe contains nearly only gas in that section. From this gamma scan, we know that the plugs were not uniform. Instead of considering the plug to be uniform, as required by *Darcy's law*, we can consider the plug to be a series of plugs with different permeabilities, as shown in Figure 3.1-5.

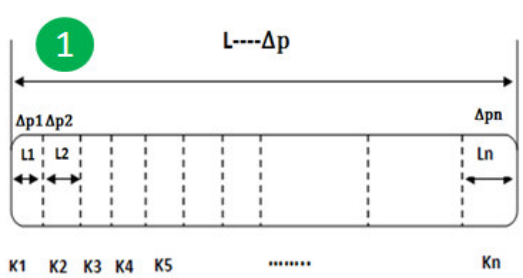

Figure 3.1-5: Permeability Distribution along the Plug

The permeability of each segment is given in Equation 3-2, and the overall permeability is in Equation 3-3, which is equal to the permeability calculated from Equation 3-1.

$$k_n = \frac{v_n \, \mu \Delta l_n}{\Delta p_n} \quad (3-2)$$

$$k_{overall} = \frac{L}{\frac{l1}{k1} + \frac{l2}{k2} + \frac{l3}{k3} + \cdots + \frac{ln}{kn}} \quad (3-3)$$

For these hydrate plugs, the lowest permeability dominates the overall permeablity. To illustrate this, assume a plug is 65 *ft* length where the first 2 *ft* holds the differential pressure of 50 *psi*. For the rest of the plug (63 *ft*), the differential pressure is only 0.1 *psi* due to a gas channel through the whole plug. For a gas flow rate of 0.2 *lb/min*; k_1 = 95 *mD* and k_2 = 1,500,000 *mD* where the overall permeability $k_{overall}$ = 3083 *mD*. However, due to the limitation of the facilities, we can not measure the pressure drop of each small section in the flow loop. What we can measure is the differential pressure over the entire 65 *ft* length or around the *U*'s length and the overall permeability.

Case 2: Bridged or not:

Figure 3.1-6 shows data for a non-bridged case of hydrate formation during pumping test. In this traces, the density inside the pipe is only about 0.5 *g/cc* which indicates the pipe is only about half full during that time.

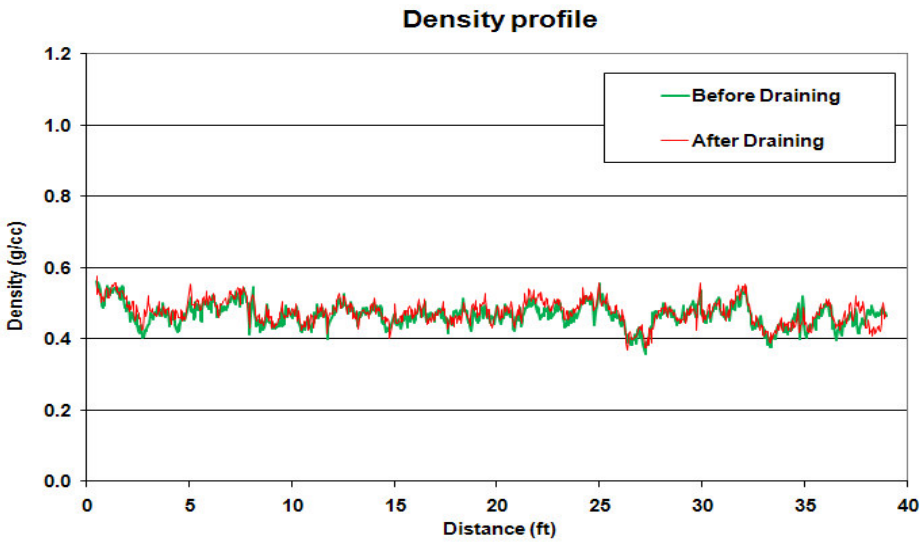

Figure 3.1-6: Density Trace along the Pipe for HYD2008-014—Nonbridged

As shown in Figure 3.1-7, case 2, the pipe is not always fully blocked by the hydrates. In this case the permeability measured is equivilant to that of an open pipe; resulting in very large values of permeability (up to 16,000 *Darcys*). In this case, we form only hydrate deposits but not a hydrate plug.

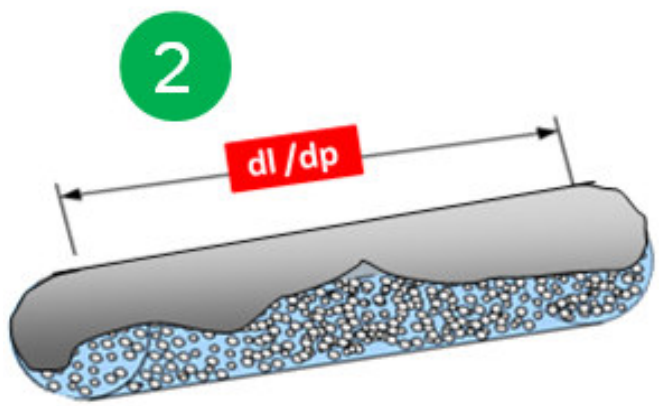

Figure 3.1-7: Non-bridged Case of Pumping Test during Measurement

Case 3: Gas Channel

As shown in Figure 3.1-8, case 3, there is a gas channel in the pore space of the plug. In this case the pores do not restrict the gas flow through the hydrate. The pores are

bypassed because the gas flows predominately through the gas channel. Thus, pressure drop readings will be small resulting in large values of permeability.

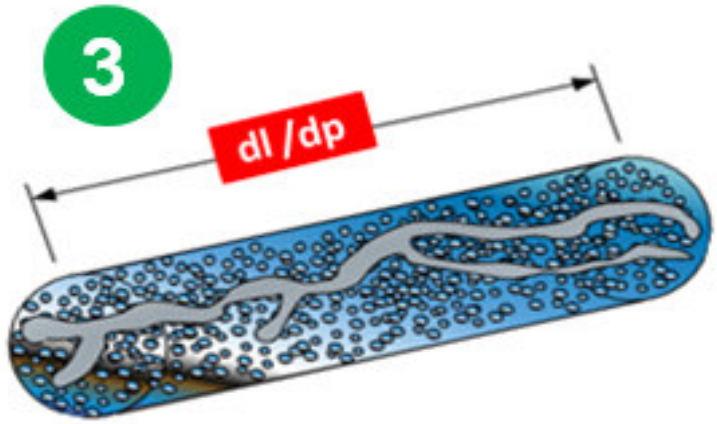

Figure 3.1-8: Gas Channel Case of Pumping Test during Measurement

Case 4: Unknown Length/ Location

It was difficult to estimate the length of the plug formed since plugs did not always form at the desired location. Figure 3.1-9 shows the possible deposit positions in the flow loop for this scenario. Of all the hydrate deposits made by pumping, there were only two cases where an impermeable hydrate plug formed: one under the gamma scanning zone and the second one in the *U* or the other leg. Another issue is that the differential pressure measured was between the two view ports which is 65 *ft* rather than the 39 *ft* that the gamma scanner scans. As a result, there is 20 *ft* ahead of gamma scanning zone and 5 *ft* after the gamma scanning zone where plugs could exist but could not be detected. These tests permeabilities from 0 to 65 *D* were determined as shown in Table 3.1-1.

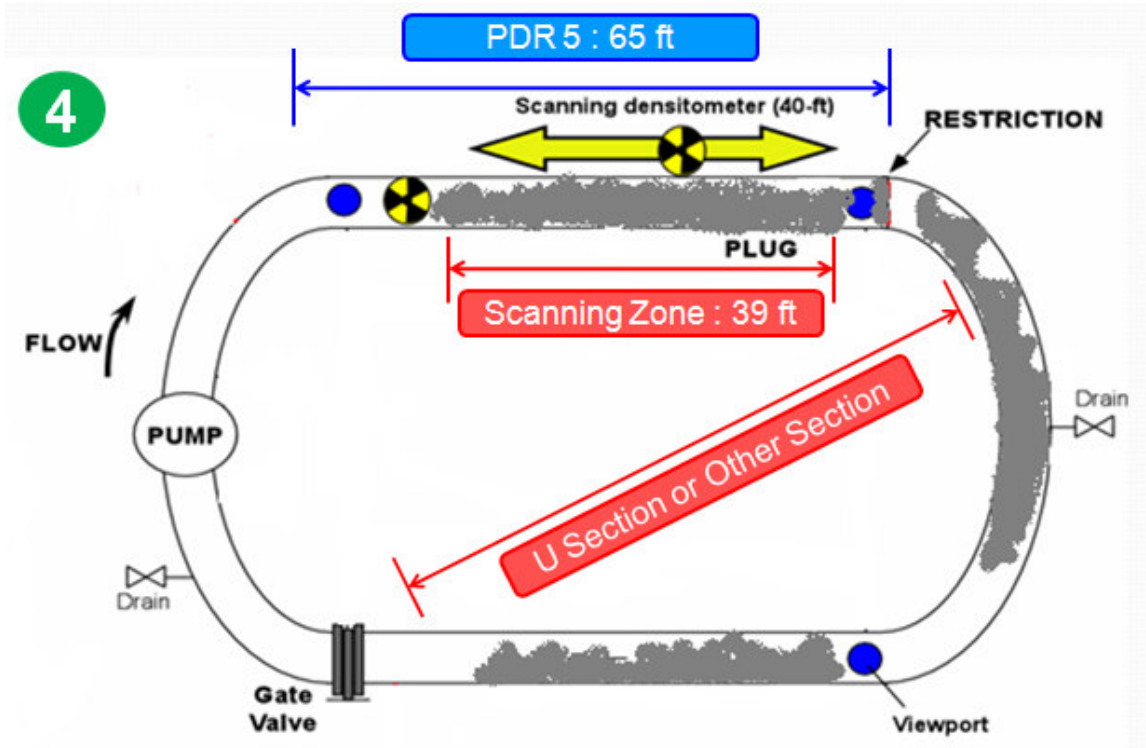

Figure 3.1-9: Possible Hydrate Locations of Pumping Test during Measurement

Porosity Calculations:

Porosity is one of the most important hydrate characteristic as well as a significant parameter for hydrate dissociation model input. It is calculated using density of the hydrate by gamma scan by Equation 3-4 based on the assumption that liquid could be drained after the plug was made.

$$\rho_{gamma} = (1-\phi)\rho_{hydrate} + \phi\rho_{pores} \Rightarrow \quad \phi = \frac{\rho_{gamma} - \rho_{hydrate}}{\rho_{pores} - \rho_{hydrate}} \qquad (3-4)$$

In Equation 3-4, ρ_{gamma} is taken from gamma densitometer scan; $\rho_{hydrate}$ is calculated from *PVT-Sim* for the given gas composition under a certain pressure and temperature; ρ_{pores} is the gas density under same pressure and temperature (in most

cases 1500 *psi* and 40 ^{o}F). In many cases, this calculation from the gamma densitometer data was usually not feasible because the liquids could not be drained from the hydrate slurry. Hence, the porosity was calculated from the density trace of the hydrate and trapped fluids, not the density of the hydrate alone. The hydrate plugs did not always form under the density scanning zone. They might form in other sections of the pipe as well, which means that density traces are not always representative of the entire plug. Since these measurements were neither reproducible nor representative of hydrate plugs formed when pumping, the next series of tests made plugs simulating a leaky valve.

3.1.3 Low Spot Tests

In the previous 18 pumping tests, porosity measurements were not successful and permeability measurements had a lot of uncertainties. In order to improve the method of obtaining porosity and permeability data, the low spot test configuration was utilized to make hydrate plugs under the gamma scanning zone with a known length. Liquids were easy to drain in this configuration resulting in porosity measurements of the hydrate deposited. The main uncertainty in the permeability measurements of the low spot tests was caused by gas channels. As the low spot tests generated better data, flow characteristic is investigated as well to study hydrate formation as a function of gas injection rate.

Permeability Calculations:

Permeability calculations were conducted using the same approach that was used for the previous pumping tests. The only uncertainty in the permeability measurement

was due to gas channels. After the plug was formed in the low spot configuration, density measurements were taken. Gas was circulated through the plug; differential pressure and gas flow rate were measured. In the hydrate formation test, two gas injection rates were adopted, which were 0.2 *lb/min* and 2 *lb/min*. The gas system described in Section 3.1.2 was used when 0.2 *lb/min* of the gas injection rate was selected. In this system, the cylinder was changed around every 10 minutes which caused the pressure fluctuations. Shown in Figure 4.1-10, permeability reduced as gas was injected into the system, and the minimum permeability in this test was 10 *D*.

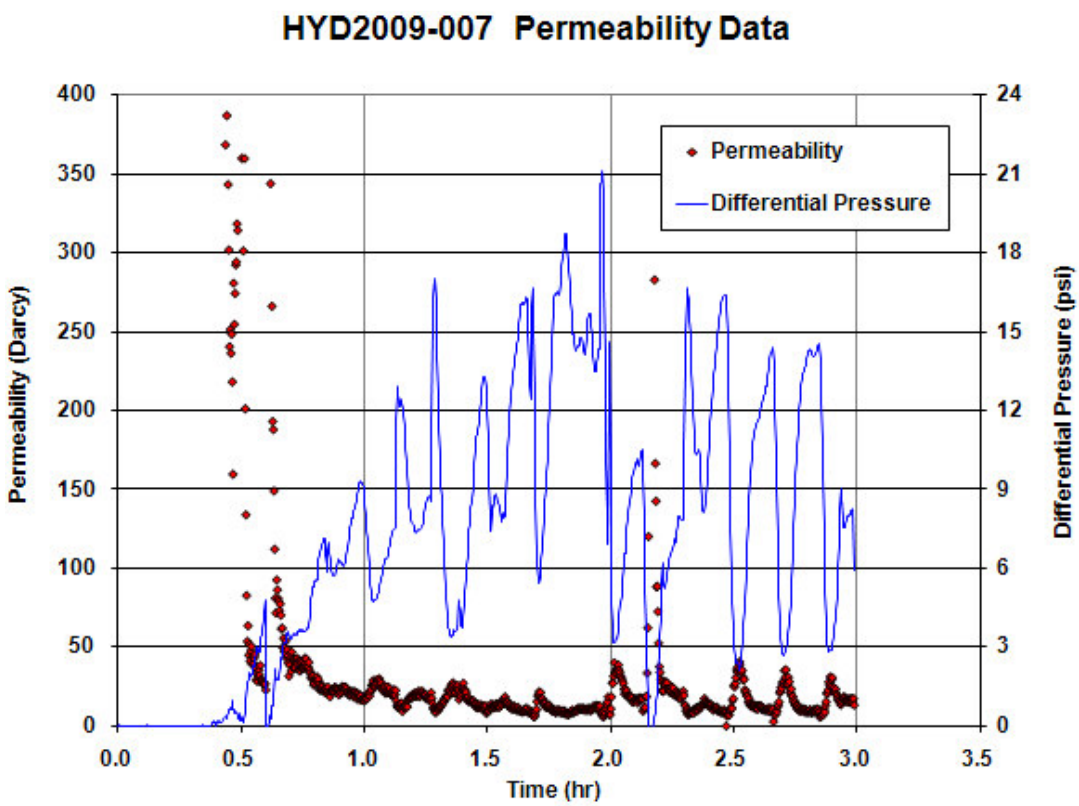

Figure 3.1-10:Differential Pressure & Permeability—HYD2009-007

The CNG system was used when the gas injection rate of 2 *lb/min* was selected. In this system, the system unloaded every 45 minutes which caused a pressure pulse to the system with the same period. Because of the pressure pulse, the hydrate plug was

compressed and became even denser. As the gas flowed through the hydrate plug, the differential pressure across the plug built up step by step and thus permeability dropped step by step. See Figure 3.1-11.

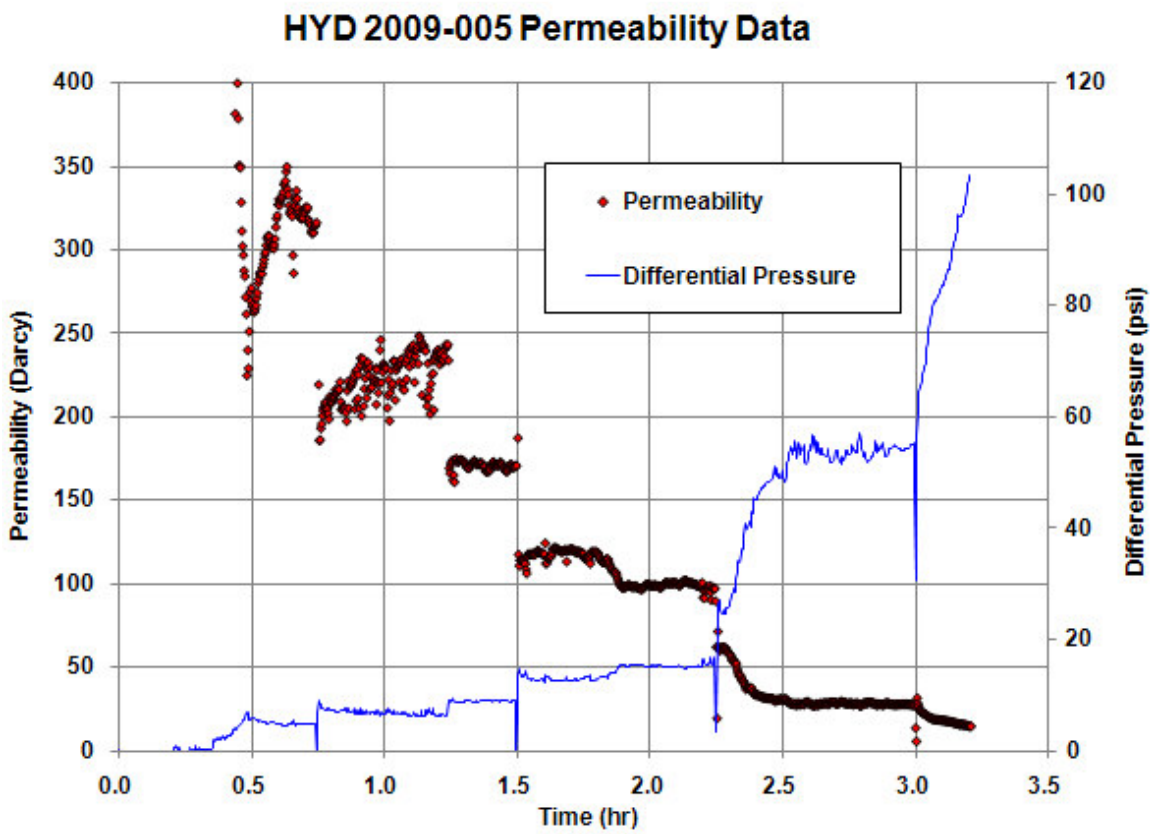

Figure 3.1-11:Differential Pressure vs. Permeability—HYD2009-005

Formation time is the total gas injection time. In most of the tests, gas injection was stopped by reaching the maximum safety differential pressure built on the plug or by the time the plug collapsed. Minimum measured permeability of low spot tests ranged from 2 *D* to 15 *D*. Permeability was also found to be a function of formation time decrease as the formation time increase, shown in Figure 3.1-12. The permeability was found to decrease with time when only gas saturated with water was flowing through the plug. It is hypothesized that these plugs would have become impermeable to gas if the gas flow was continued for a longer duration, as is indicated in Figure 3.1-12.

Permeability data are summarized in Table 3.1-2. However, gas injection was continued to the flow loop after the plug collapsed in very few of the cases. Formation time in parentheses is the few cases with continued gas injection, the value inside the parentheses is the time from gas injection to the time which minimum permeability was reached. Permeability data of HYD2009-006 and 019 were not shown because of a gas channel and thus the permeability were huge and not representitive.

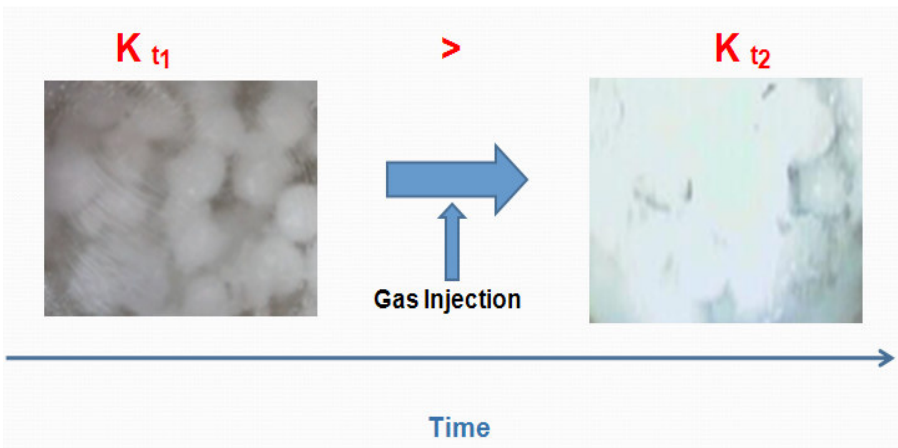

Figure 3.1-12: Hypothesis—Plug Became Impermeable for Longer Gas Injection

Table 3.1-2: Low Spot Experiments Permeability Data

Test #	Gas Injection Rate lb/min	Salinity %	Sub Cooling F	Formation time hr	Minimum Permeability Darcy
HYD2009-013	0.2	0	5	5.5	No Plug
HYD2009-012			10	4.2	6
HYD2009-003			21	4	5
HYD2009-011		14	7	14	No Plug
HYD2009-010		7	15	4.4	3
HYD2009-009				3.9(2.1)	9
HYD2009-015		3.5	10	7.2	2
HYD2009-014			11	6.5	2
HYD2009-008			18	3	7
HYD2009-007				3(2.6)	10
HYD2009-018	2			1.5	8
HYD2009-016				4	6
HYD2009-005				3.2	15
HYD2009-004		0	21	1.6	12

Scale-up:

Minimum permeabilities calculated from low spot tests range from 2 *D* to 10 *D* based on 39 *ft* of plug length and 0.2 *lb/min* gas injection rate, and 6 *D* to 15 *D* on 2 *lb/min* gas injection rate. Considering this scenario in fields, assuming 1 mile of plug length with 2 *D* to 10 *D* range of permeability and 0.2 *lb/min* of gas circulation, the pressure drop build up across the plug will be 6273 *psi* to 1255 *psi*. With such a huge pressure drop, there no way gas could flow in the field.

Hydrate Formation:

Hydrate formation time is basically our gas injection time until maximum pressure drop was reached or the plug collapsed. As shown in Table 3.1-2, hydrate formation time is a function of sub-cooling temperature, salinity and gas injection rate.

At the same gas injection rate and salinity, larger sub-cooling shortened formation times, which is reasonable because larger sub-cooling brought a larger driving force while forming hydrates. Take HYD2009-007, 008, 014 and 015 for example, with the same salinity and gas injection rate: sub-cooling for HYD2009-007 and 008 was 18 ^{o}F and for HYD2009-014 and 015 was around 10 ^{o}F. With around 8 ^{o}F less sub-cooling temperature, HYD2009-014 and 015 needed more than two times of formation time of HYD2009-007 and 008.

At the same gas injection rate and sub-cooling temperature, larger salinity extended the hydrate formation time. Take HYD2009-015 and 012 for example, with the same sub-cooling temparture and gas injection rate: salinity for HYD2009-015 and 012 was 3.5% and 0% respectively. HYD2009-015 took around 7 hours to form the hydrate plug and HYD2009-012 took around 4 hours to form the hydrate plug. HYD2009-007

008 and 003 shared the same gas injection rate and similar sub-cooling temperature with different salinities; however, HYD2009-003 took longer to form hydrates than HYD2009-007 and 008. So in this case, the data are inconclusive.

At the same salinity and sub-cooling temperature, faster gas injection rate shorten the hydrate formation times. Take HYD2009-003 and 004 for example, with the same sub-cooling temperature and salinity, HYD2009-004 took 1.6 hours to form hydrate while HYD2009-003 took 4 hours. However, the same trend could not get from HYD2009-016 with HYD2009-007. So the data are inconclusive here as well.

Hydrates plugs formed in the low spot experiments were also found to be reproducible. See Figure 3.1-13 for permeability data during formation time. HYD2009-007 and 014 were conducted using the same operating conditions except for sub-cooling temperature, which were 18 ^{o}F and 11 ^{o}F for HYD2009-007 and 014, respectively. Formation times for HYD2009-007 and 014 were 2.6 and 6.5 *hrs* respectively.By arbitarily shifting the permeability data for HYD2009-007 for 2 *hrs* behind the permeability trends were almost identical.

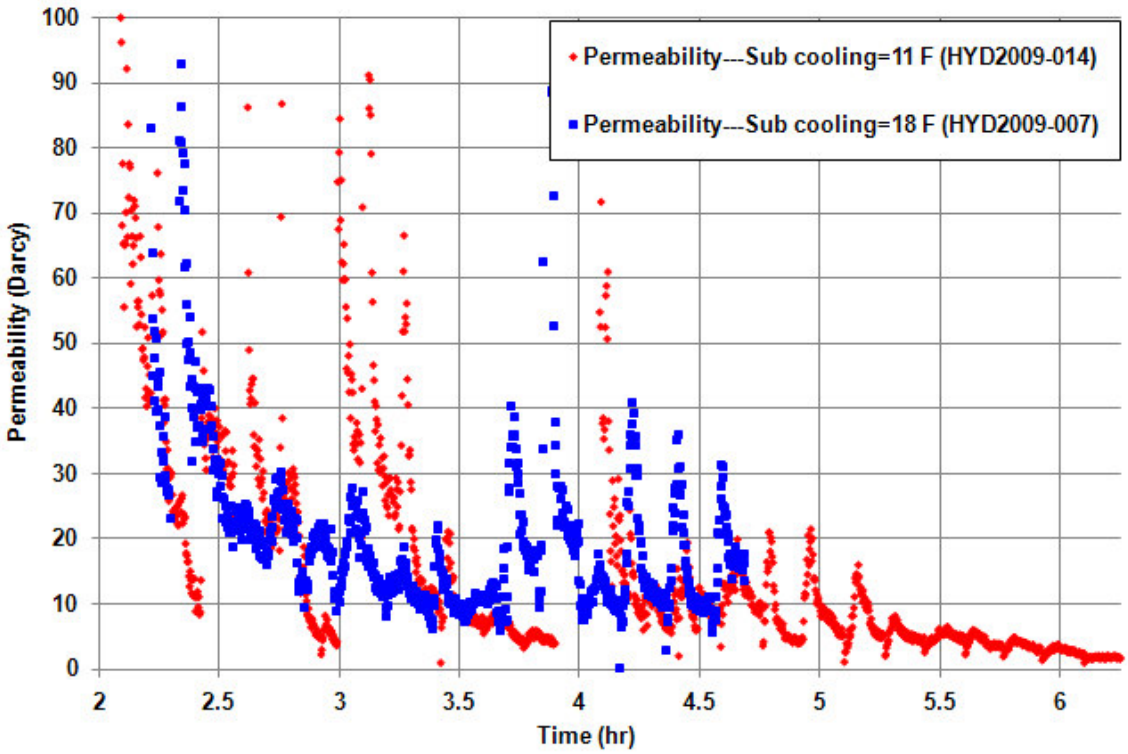

Figure 3.1-13: Reproducibility of Hydrate Plugs for HYD2009-007 and HYD2009-014

Porosity Calculations:

For the low spot tests, the hydrate plug was located under the gamma scanned zone and water could be drained. So the porosity calculated from the gamma scan is therefore representive of the hydrate inside the flow loop. Before dissociation, water was drained and several gamma scans were taken to measure the density of the hydrate plug so porosity could be calculated. Assuming that the pipe is filled with only hydrates after draining and the pore space is filled with gas, porosity is calculated as:

$$\phi = \frac{\rho_{hydrate} - \rho_{gamma_scan}}{\rho_{hydrate} - \rho_{gas}} \qquad (3-5)$$

Porosities are reported in Table 3.1-3 sorted by different gas injection rates. From the results shown in Table 3.1-3, the hydrate porosity in the low spot tests is repeatable and ranges from 0.70 to 0.86. This range of porosity data matches the hydrates observed in field, which is very porous.

Table 3.1-3 Low Spot Experiments Porosity Data

Test #	Gas Injection Rate lb/min	Salinity %	Sub Cooling F	Porosity
HYD2009-013	0.2	0	5	0.86
HYD2009-012			10	0.80
HYD2009-003			21	0.80
HYD2009-011		14	7	0.81
HYD2009-010		7	15	0.79
HYD2009-009				0.84
HYD2009-015		3.5	10	0.82
HYD2009-014			11	0.70
HYD2009-008			18	0.86
HYD2009-007				0.77
HYD2009-006				0.76
HYD2009-019	2			0.79
HYD2009-018				0.70
HYD2009-016				0.82
HYD2009-005				0.82
HYD2009-004		0	21	0.71

Flow Characteristic:

The flow characteristic of a control valve is the relationship between control valve capacity and stem travel. Flow characteristic is introduced as a function of hydrate onset and gas injection volume with low gas injection rate or low gas leaking rate. Hydrate onset is defined as when the hydrate particles are large enough to cause noticeable pressure drop of 1 *psi*.

According to the definition of flow coefficient of a control valve, flow rate is equal to flow coefficient times flow characteristic times the square root of pressure drop

divided by g_s (g_s is specific gravity of the fluid, also a fixed value in certain experiments), see Equation 3-6.

$$q = C_v \cdot f(l) \cdot \sqrt{\frac{\Delta p}{g_s}} = \beta \cdot \ C_v \cdot f(l) \cdot \sqrt{\Delta p} \quad \left(\beta = \sqrt{\frac{1}{g_s}}\right) \quad (3-6)$$

According to *Darcy's* Law, flow rates have a certain relationship with permeability which is shown in Equation 3-1.

$$q = \frac{k\,A}{\mu}\frac{\Delta p}{\Delta l} \Rightarrow k = \frac{v\,\mu \Delta l}{\Delta p} \quad (3-1)$$

As the fluid viscosity, the plug length and the area are fixed values in the same experiment as well, Equation 3-1 can be also written as Equation 3-7.

$$k = \alpha \cdot \frac{q}{\Delta p} \quad \left(\alpha = \frac{\mu \cdot \Delta l}{A}\right) (3-7)$$

After rearrangement of Equation 3-6 and 3-7, flow coefficient times flow characteristic was found to be directly proportional to permeability times the square root of pressure drop, see Equation 3-8.

$$k = \gamma \cdot \frac{C_v \cdot f(l)}{\sqrt{\Delta p}} \quad (\gamma = \alpha \cdot \beta) \quad (3-8)$$

In order to get a relationship of flow characteristic as a function of gas injected, 1 *GPM psi* was chosen as the flow coefficient C_v value. Flow characteristic as a function of gas injected was calculated and plotted in the following figures. The horizontal axis represents a dimensionless value which is the volume of gas injected divided by the total volume of the flow loop. The vertical axis represents the flow characteristic, in which a value of one indicates no restriction to the flow and the value zero indicates no flow. In order to compare with the control valve characteristic plot, the horizontal axes are shown

in reverse order. This indicates that once hydrate started to form, the area available flow for deteriorates rapidly, much like an equal-percentage valve.

Figure 3.1-14 shows the flow characteristic of HYD2009-007 and 008 which share the same gas injection rate of 0.2 *lb/min*. Hydrate onset appeared at 0.2 flow loop volume of gas injected with 3.5% salinity and 18 °*F* of sub-cooling temperature.

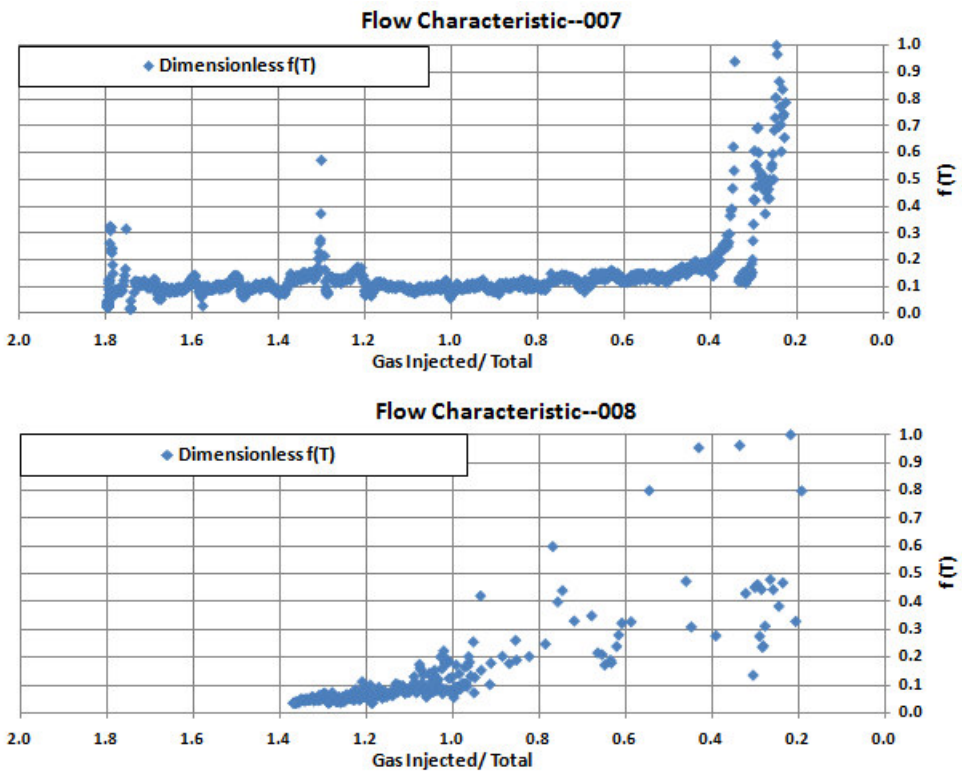

Figure 3.1-14 Flow Characteristic—HYD2009-007 and HYD2009-008

Figure 3.1-15 shows the flow characteristics of HYD2009-014 and HYD2009-015, in which hydrate appeared at 1.0 flow loop volume of gas injected with 3.5% salinity and 10 °*F* of sub-cooling temperature.

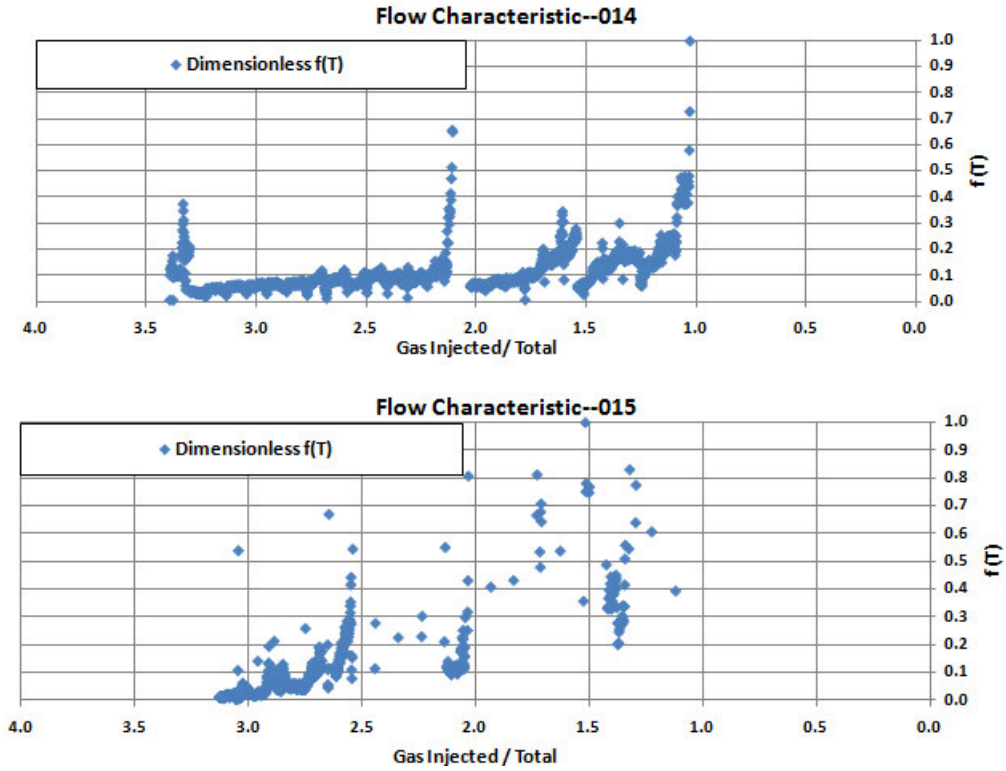

Figure 3.1-15 Flow Characteristic—HYD2009-014 and HYD2009-015

This result is reasonable because lower sub-cooling temperature gives small driving force to form hydrate in the same condition and slows the formation rate. Also this result gives a reference on hydrate onset as a function of gas injection volume on low gas injection rate or low gas leaking rate. These results could be used for hydrate onset predictions.

3.2 Hydrate Dissociation Studies

All 18 hydrate plugs from the pumping tests were dissociated by heating. In most cases, the flow loop was heated to 70 °*F* or higher directly. Due to the large driving force (in most cases more than 15 °*F*), the hydrate plugs dissociated very quickly (in 1 to 2

hours) and the hydrate plugs suddenly collapsed and thus caused the end of the experiment, as shown in Figure 3.2-1.

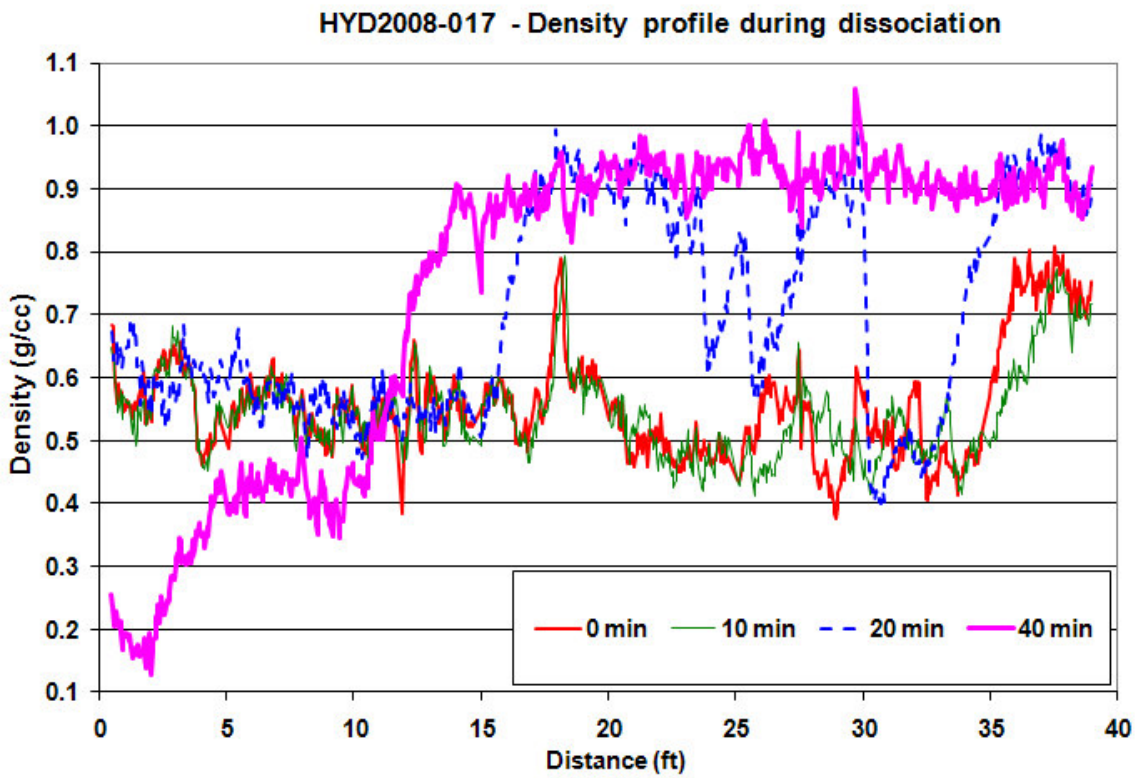

Figure 3.2-1: Hydrate Density Profile during Dissociation--HYD2008-017

The scans at 0 and 10 minutes show that most of the pipe is filled with hydrates with a density of about 0.6 *g/cc* with a more dense section around 35 *ft*. After 20 minutes of increased loop temperature to 70 °*F*, the density is higher in the 15 to 30 *ft* section. This could be because the hydrate plug collapsed and moved to the lower side of the pipe (right side of the chart), yielding a compacted plug in the 15 to 30 *ft* section. Or the plug could be dissociating with water accumulating in the pipe. The scan at 40 minutes indicates that water has filled the pipe from 15 to 40 *ft*. In the later low spot tests, the heating dissociation was done with a smaller driving force such as one or two degrees

above the dissociation temperature. This lower driving force gave better dissociation trends and results (shown in Figure 3.2-3 later in the low spot test results).

3.2.1 CSM Model Selection

Two possibly appropriate models in *CSM-Plug* are available: two sided depressurization and electrical heating. Both modes were used to model the pumping test dissociations.

The two sided depressurization model requires the outside heat transfer coefficient h_0. We calculated h_0 with Pethukov-Kirillov correlations, yielding 250-300 $Btu/hr.ft^2 °F$. For the direct heating model, the heat input was estimated from the heat loss of the glycol flowing in the pipe annulus, as shown in Equation 3-9:

$$\frac{Q}{L} = \frac{\dot{m}_{glycol} C_P \left(T_{in,glycol} - T_{out,glycol}\right)}{L} \qquad (3-9)$$

The heat loss from glycol is around 250 *W/m*, but this value is not accurate for the following reasons:

- The glycol temperature difference from inlet to outlet is very small, 1 to 2 °*F*.
- The glycol temperature oscilates, which complicates the calculation of the temperature difference.
- The range of calculated *Q/L* is large.

Simulations were conducted with different values of the overall heat transfer coefficient within a range of 200 $Btu/hr.ft^2$ °*F* to 400 $Btu/hr.ft^2$ °*F* and the simulation results were the same. This is interpreted to mean that the dissociation is not heat-

transfer limited. Simulation results with the two different models are shown in Figure 3.2-2.

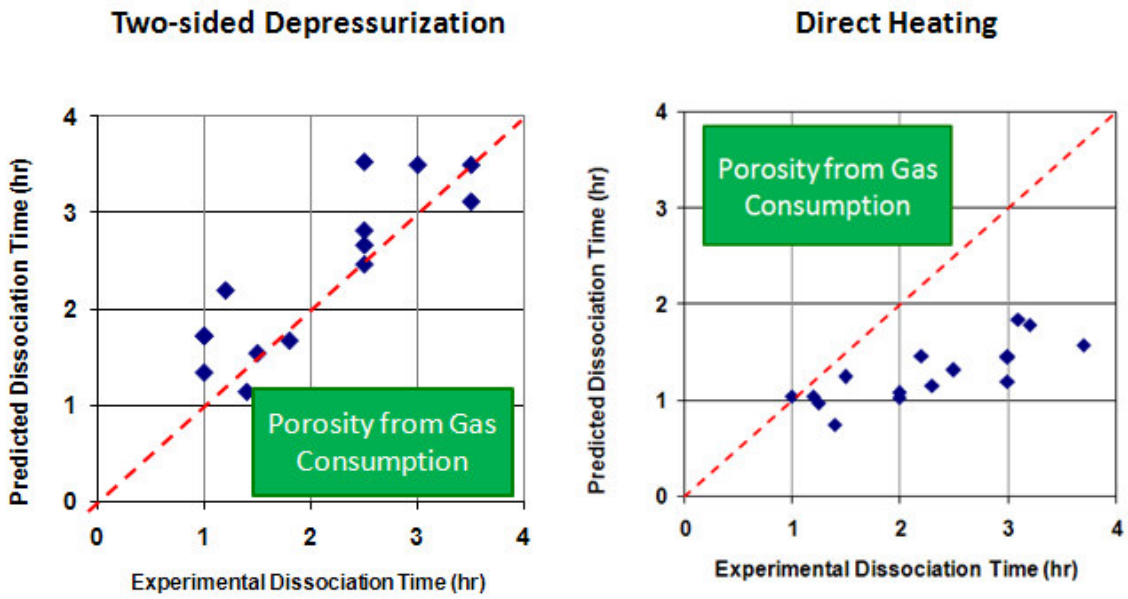

Figure 3.2-2: Simulation Results for Pumping Experiments Using Two-sided Depressurization and Direct Heating

Because liquid was not able to be drained after the hydrate formation pumping experiments, porosity could not be calculated correctly form the density scan. However, porosity is one of major inputs in *CSM-Plug* to represent hydrate portion in dissociation simulation. So the porosity input in the dissociation model is calculated by gas consumption. The hydrate volume was calculated based on how much gas was consumed in the experiments. The porosity input in the model is the hydrate volume divided by the total pipe volume. However, in many of the hydrate deposits, the hydrate did not fill the entire pipe. This porosity from gas consumption assumes the hydrate does fill the pipe, so these porosities are not representative of the true hydrate porosity. The porosities were used only as a model input to indicate how much hydrate to dissociate.

From analyzing the experimental data and observing the charts, the decision was made to use the two-sided depressurization model as our model and porosity calculated from gas consumption as our input to the model. Our input parameters for the two-sided depressurization model are more reliable and thus yield better results than the direct heating model.

3.2.2 Dissociation Methods

Of all the 16 low spot hydrate dissociation tests, 13 of them were dissociated with both constant heating or stepped heating, 4 of them were remediated with depressurization, and one of them were dissociated with inhibitor of MEG. One example of each method is discussed to illustrate the dissociation experiments; however, the dissociation test information is summarized in Table 3.2-1. This table summarized the dissociation test methods, hydrate plug salinity, dissociation driving force, porosities for model input and the inclination angle during dissociations. The driving forces from the depressurization tests are displayed as temperatures. These temperatures are translated from pressures from the hydrate equilibrium curve. The driving forces from the inhibitor tests are dependent on the inhibitor concentrations. The driving forces from the heating dissociation tests range from 2 to 5 °*F*. The inclination angles for all the dissociation experiments varied from -8 to 2 degrees. The variations of the inclination angles were due to adjustments made to find the perfect dissociation angle. Inclination angles larger than +/-2 degree caused the hydrates to slip down to the lower end of the pipe during dissociation. Inclination angles smaller than +/-2 degree did not allow water to drain during dissociation. So finally, +/- 2 degree was chosen as the inclination angle for dissociation. After test 12, all dissociation tests were performed using an inclination angle

of -2 degree except test 16. However, after all the data were processed, water dissociated from the hydrates on the top (pump side) was found. In order to avoid this mass increase in the data, inclination angle of +2 degree is recommended in the future tests.

Table 3.2-1 Dissociation Test Information

Dissociation Method	Salinity (%)	Driving Force (^{o}F)	Porosity	Inclination Angle (Degree)	Test #
Heat	3.5	3	0.76	1	HYD2009-006
	3.5	2	0.77	-2	HYD2009-007
	3.5	4	0.86	-3	HYD2009-008
	7	2	0.84	-3	HYD2009-009
	7	5	0.79	-3	HYD2009-010
	14	2	0.81	-3	HYD2009-011
	0	3	0.80	-2	HYD2009-012
	0	-	0.86	-2	HYD2009-013
	3.5	-	0.70	-2	HYD2009-014
	3.5	2	0.82	-2	HYD2009-015
	3.5	3	0.79	-2	HYD2009-019
Depressurization	0	3	0.80	-8	HYD2009-003
	0	8	0.71	-4	HYD2009-004
	3.5	5	0.82	-8	HYD2009-005
	3.5	4	0.82	2	HYD2009-016
MEG	3.5	Depends on Concentration	0.70	-2	HYD2009-018

*HYD2009-013 did not conduct dissociation test because no hydrate plug was formed
*HYD2009-014 did not finish dissociation test because gamma chain broke during the test

After all the data processed of the low spot test, a dissociation procedure was developed to dissociate hydrates. An inclination angle of +2 degree was needed to allow the water to drain and yet prevent the plug from collapsing when first starting to dissociate. Density traces were taken every 10 to 15 minutes to get the mass change. After a step in temperature (heating) or pressure (depressurization), another step was not

taken until integration of the gamma scan mass stabilized. Water was drained when observed at the lower view port to prevent the water accumulation under the density scan.

Heating:

Density traces for dissociation by heating are shown in Figure 3.2-3**.** In this dissociation, the driving force is 2 °*F* during dissociation and a uniform decrease in density along the length of the gamma densitometer was seen during the dissociation.

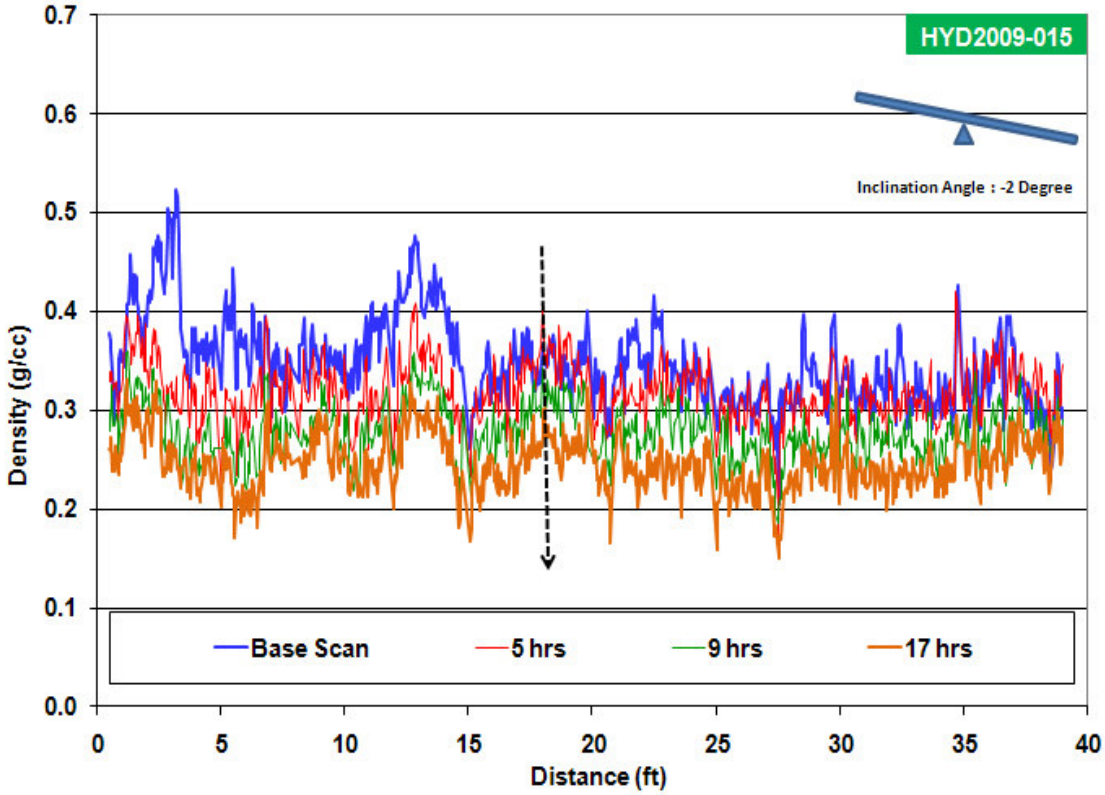

Figure 3.2-3: Density Traces for Heating Dissociation--HYD2009-015

Depressurization:

The depressurization tests conducted did not show the uniform dissociation observed with the heating dissociation test**.** Figures 3.2-4 and 3.2-5 show density traces

during depressurization dissocation. The shaded areas are where the density did not change as it did as the rest of the pipeline. Some possible explanations for this observation might be plug collapse while dissociating, water accumulation or ice formation. In addition, the assumption for the depressurization model is that the plug is very porous and the pressure is able to distribute itself along the plug. However, the pressure is not evenly distributed in the hydrate plug we made. The loop pressure reduced suddenly and built back up which indicated that pressure was not evenly distributed during depressurization. This might be another contribution to the non-uniformly dissociated hydrate plugs.

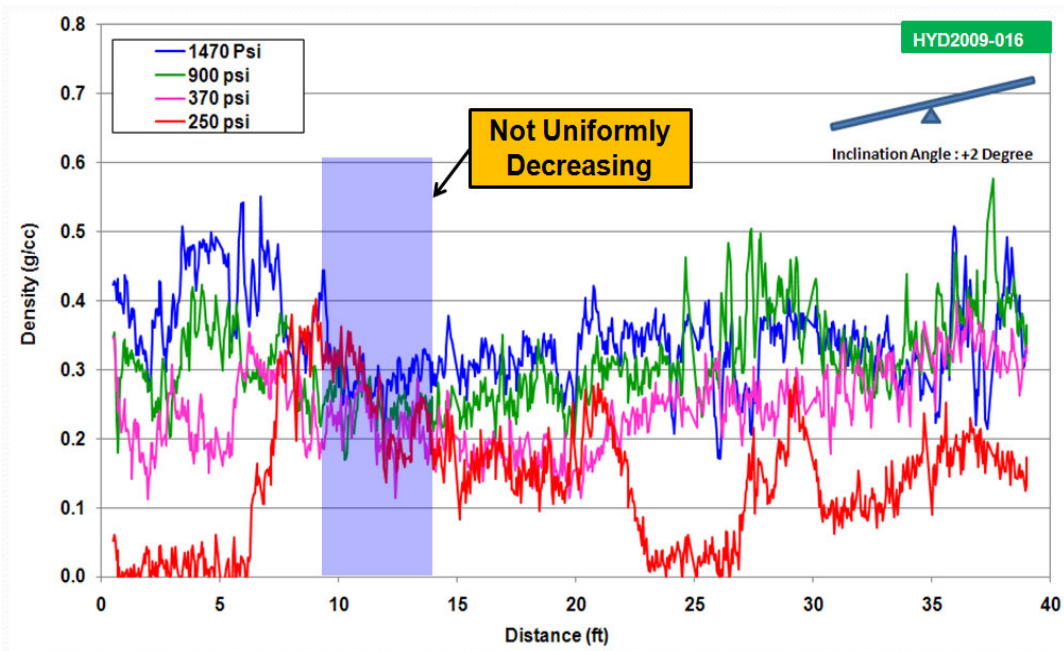

Figure 3.2-4: Density Traces of Depressurization Dissociation—HYD2009-004

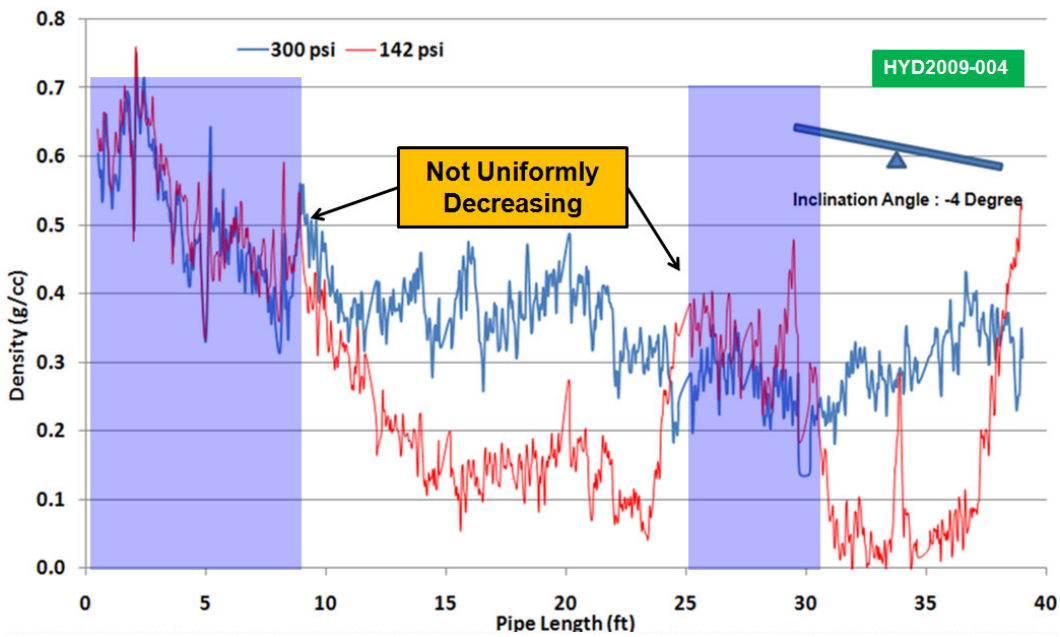

Figure 3.2-5: Density Traces of Depressurization Dissociation—HYD2009-016

MEG:

Figure 3.2-6 shows density traces inside the pipe before MEG injection, at maximum MEG injected, and after liquid draining which are marked as blue, green and red respectively. After MEG was injected into the system at a rate of 0.1 *GPM*, the density increased in many areas. The shaded areas in Figure 3.2-6 with density around 1.0 *g/cc* indicate that MEG was in that area of the hydrate. In the same areas, after draining the fluids, the density does show a drop from the base scan because these areas were in contact with MEG and did dissociate. As the hydrate dissociated, eventually the hydrates formed a bridge in the middle of the view port, with gas on top and glycol flowing at the bottom. The hydrates in the middle were not in contact with MEG and did not dissociate. In this experiment, MEG was injected at the top end of the pipe and drained at the bottom, which might cause MEG to have insufficient contact with

hydrates. In order to assure full MEG contact with hydrates, it is recommended to inject MEG from the bottom in the future experiments.

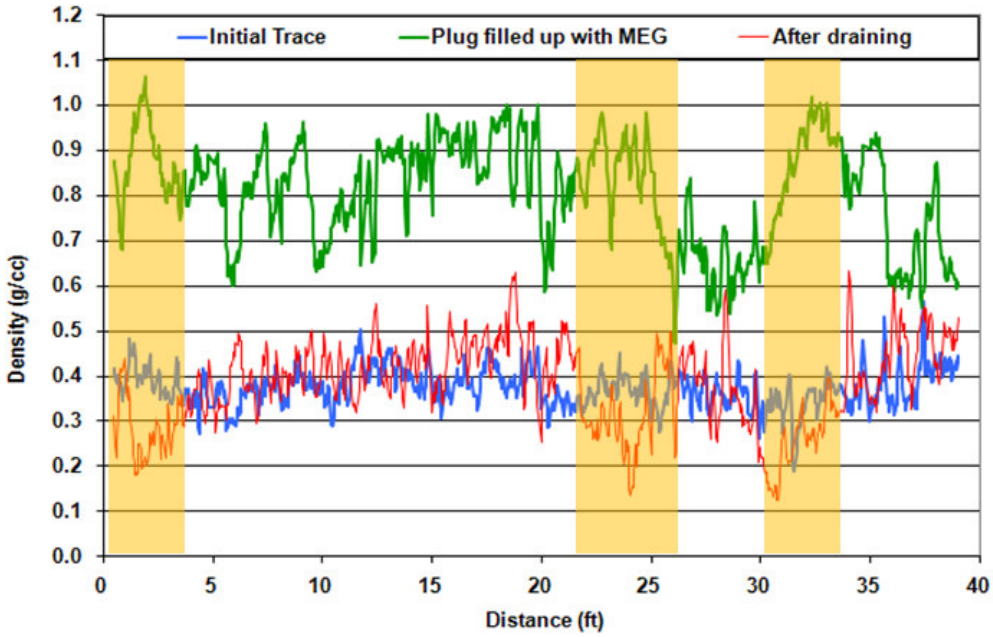

Figure 3.2-6: Density Traces of MEG Dissociation –HYD2009-018

3.2.3 Comparison of Experimental Data with CSM-Plug Simulation

Mass Calculation:

The experimental mass was calculated from density scans. Along the total scanning distance of 39 *ft*, 925 points of density were recorded. The pipe is then divided into 925 small sections. The mass inside the pipe is obtained from the integration of the density scan, see Figure 3.2-7.

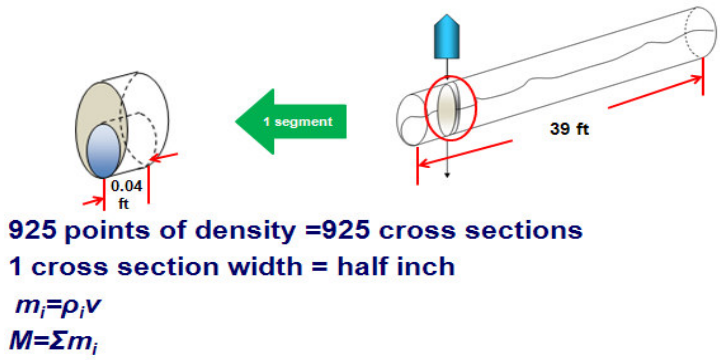

Figure 3.2-7: Density Integration—Experimental Mass

The simulation results offer a plot of hydrate radius as a function of dissociation time. With this information, the hydrate volume can be calculated. The mass of the hydrate is equal to the volume times experimental density from the gamma scan and hence the simulation mass can be calculated.

Heating:

CSM-Plug's two-sided depressurization model works well for heating dissociation when the glycol jacket temperature is constant. When the temperature is stepped during the dissociation time, *CSM-Plug* may over predict the dissociation time, depending on what "constant" temperature is entered into the program. For example, in test HYD2009-015 (see Figure 3.2-8), the temperature was raised 2 °*F* above the dissociation temperature and kept constant during dissociation. In this simulation, *CSM-Plug* works fine and captured the dissociation trend well.

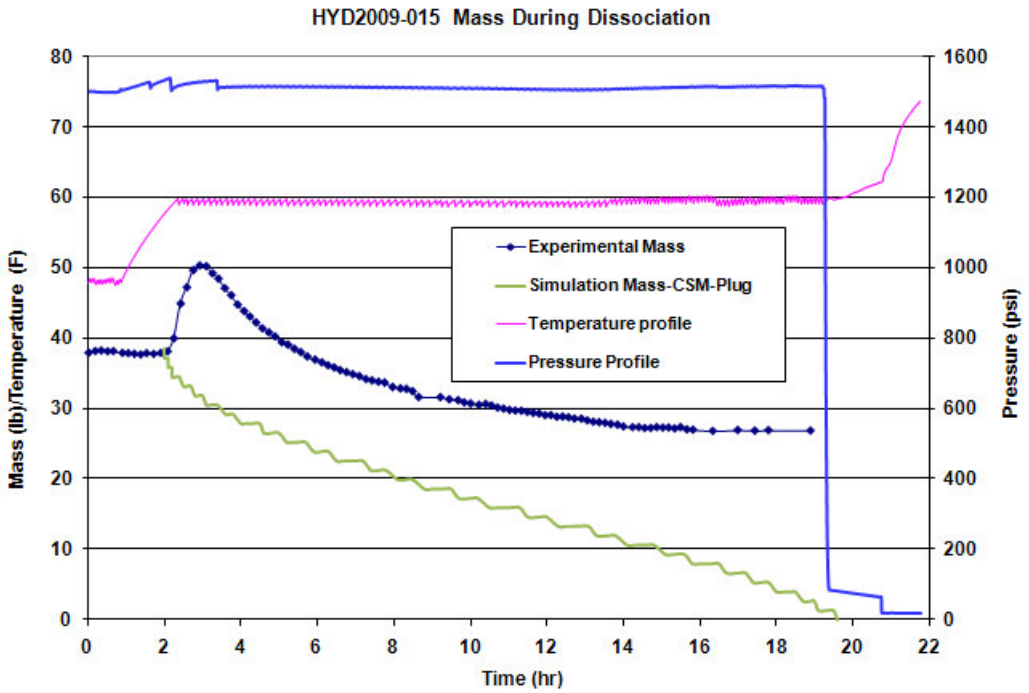

Figure 3.2-8 Simulation and Experimental Mass Change during Dissociation—HYD2009-015

But in test HYD2009-012 (Figure 3.2-9), the glycol temperature was stepped several times, and the agreement between CMS-Plug's predictions and experimental results is not as good as the previous example. In test HYD2009-012, *CSM-Plug* over predicted the dissociation time by almost 100% when the input temperature was 62.8 °*F* (Average temperature from the dissociation temperature to the temperature at the end of the experiment). The correct input must be chosen because this model does not account for temperature profile input. The correct temperature input to get the correct dissociation time was found by trial and error to be "63.9 °*F*".

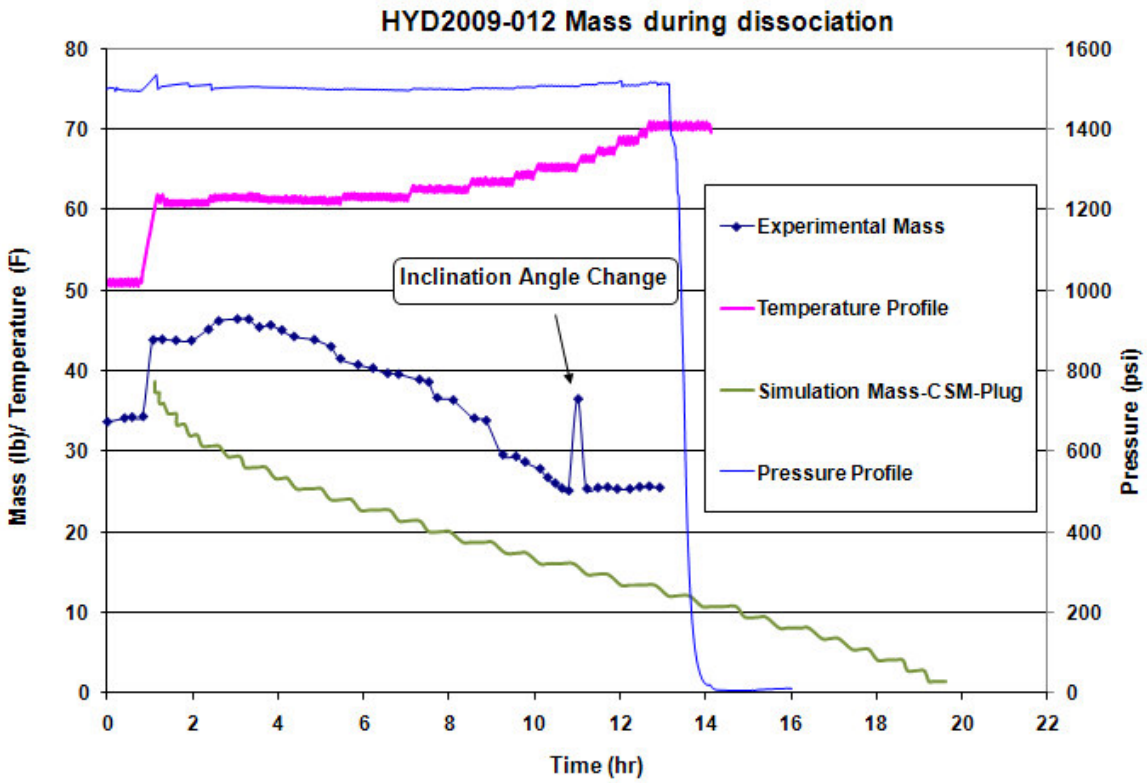

Figure 3.2-9 Simulation and Experimental Mass Change during Dissociation—HYD2009-012

Depressurization:

The *CSM-Plug* model assumes that the time to drop the pressure is insignificant compared to the time to dissociate the plug. This may be true for producing fields. Since our time to decrease the pressure in our facility is 3 hours and our dissociation time is 10 hours, this assumption is not valid for our experiments.

3.2.4 Comparison of TU Model and CSM-Plug Simulation

Heating:

In test HYD2009-015 (Figure 3.2-10), the hydrate was dissociated at constant glycol jacket temperature; *CSM-Plug* two-side depressurization and *TU*'s model give

very similar results, even when *TU*'s model takes into account temperature and pressure inputs. But at the end of the dissociation, there is a sudden dissociation when the pressure is dropped which only *TU*'s model captures. In test HYD2009-012 (Figure 3.2-11), the hydrate was dissociated by step changing the glycol jacket temperature; *CSM-Plug* apparently over predicts the dissociation time when the average temperature is used. *TU*'s model is able to handle the temperature changes and better match the experimental data.

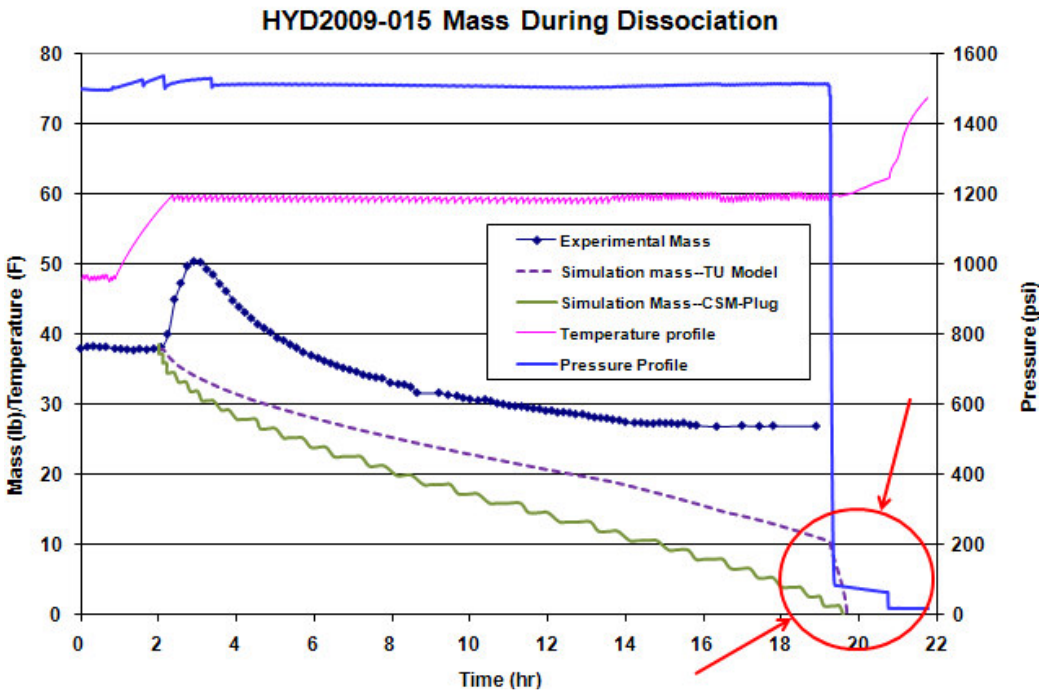

Figure 3.2-10: Simulation Comparison between *TU*'s Model and *CSM-Plug*—HYD2009-015

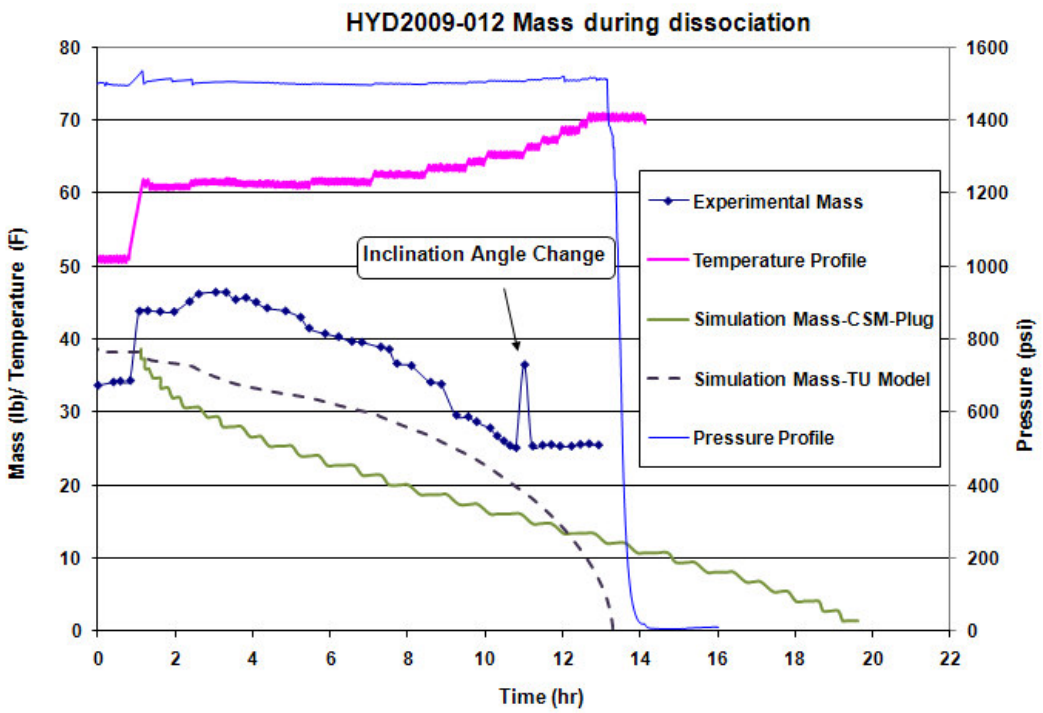

Figure 3.2-11: Simulation Comparison between *TU*'s Model and *CSM-Plug*—HYD2009-012

Since *TU*'s model has the advantage of entering a temperature profile instead of a constant temperature; *TU*'s model captures the actual dissociation process better, as seen by the changes in dissociation rate with changes in T and P in Figure 3.2-10 and 3.2-11. The dissociation times from *TU*'s model match the experimental dissociation time better than *CSM-Plug*, which over predicts the dissociation time when the input is an average temperature.

Overall Simulation Data Comparisons:

The overall heating simulated dissociation data vs. experimental dissociation data are shown in Figure 3.2-12. The *TU* model matches our experimental data better by allowing for temperature profile input. *CSM-Plug* over-predicted most of the dissociation times.

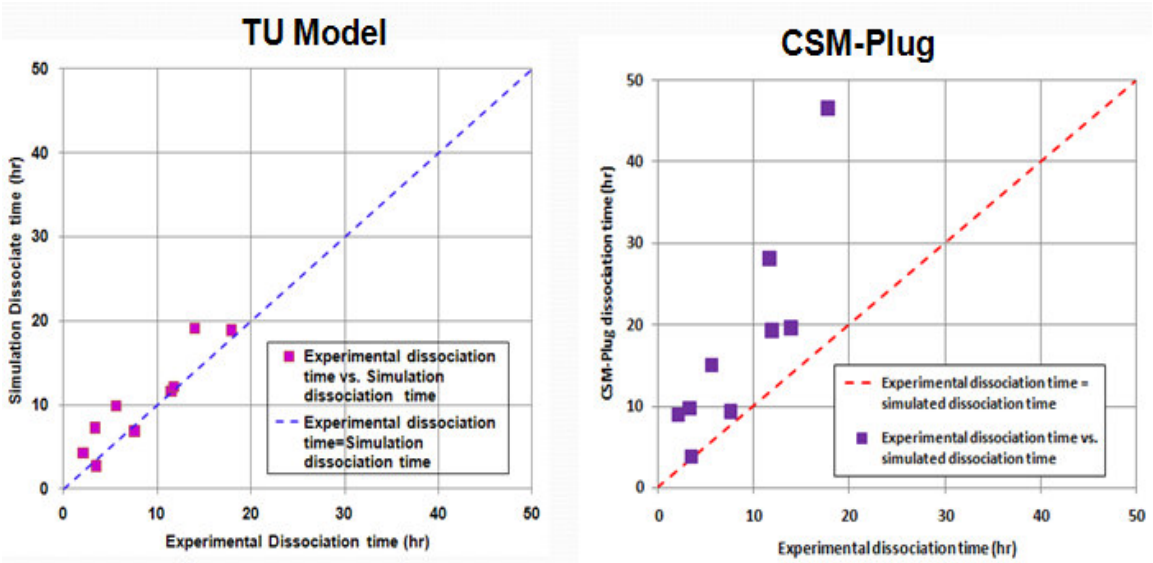

Figure 3.2-12 Simulations of Low Spot Experiments with *TU* Model and *CSM-Plug*

3.2.5 Inhibitor Model

Since no inhibitor model was available, a first generation inhibitor model was created by Dr. Ford from University of Tulsa in VBA program. It calculates the dissociation time for dissociation of a structure I methane/fresh water hydrate by MEG at 1500 *psi*. Ice formation is currently ignored. Fourier's law for heat conduction in cylindrical coordinates is used. The inhibitor flows into the cell, changing the concentration of the liquid phase, so the dissociation temperature is calculated at every time step. All inhibitor solution that has been pumped in and dissociated liquids are assumed to be mixed in the calculation area. The plan is to expand this model in a future project into a model with many cells chained together and to link the model to a thermodynamic package to allow modeling of more hydrate-forming fluids. The scheme of the simulation model is shown in Figure 4.2-13 and the instructions of calculation procedure is in Appendix F.

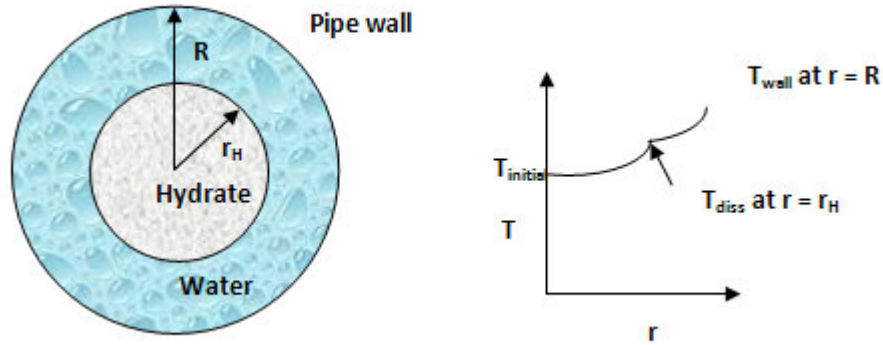

Figure 3.2-13 Scheme of Inhibitor Dissociation

Nomenclature:

R = inside radius of pipe wall

r_H = outside radius of hydrate

$T_{initial}$ = initial temperature of hydrate

T_{wall} = pipe wall temperature

T_{diss} = hydrate dissociation temperature

From the results of model comparisons above, *CSM-Plug* two-sided depressurization model is able to predict hydrate dissociation time and agrees with our experimental data when there is no pressure and temperature change during dissociation. However, when pressure or temperature changed during dissociation, *CSM-Plug* two-sided depressurization model did not agree with the experimental data. *TU* model allows the temperature and pressure profile input during dissociation, and thus yielded better simulations results. However, *TU* model does not consider ice formation during the dissociation. In the future, it is recommended to incorporate ice formation in *TU* model. The first generation of inhibitor model is developed by VBA. In future, more inhibitor

dissociation tests should be run to verify this model. In addition, the inhibitor model should be developed able to link to *PVT-Sim* for input data.

CHAPTER 4

CONCLUSIONS AND FUTURE WORK

4.1 Hydrate Characterization Conclusions

The first set of experiments on hydrate characterization were conducted with the pumping tests. However, hydrate plugs did not form where the blocking plate was located as we hypothesized and thus the hydrate permeability calculations have large uncertainties because we don't know the plug length or locations. In order to improve the method of obtaining porosity and permeability data, a second set of experiments were conducted in the low spot test configuration which produced hydrate plugs under the gamma scanning zone with a known length.

4.1.1 Pumping Tests

The expected jamming effect did not take place; rather, the plugs generated under these conditions were in fact slugs of hydrates that only stopped flowing. As a result, plugs sometimes formed after the plate, since hydrates were able to squeeze around the plate and stall downstream in the U-section. No repeatable permeability measurements were made for the tests conducted. The following conclusions and lessons learned were drawn:

- Plugs generated in the pumping experiments did not form by agglomeration as anticipated but rather consist of a hydrate slurry that stopped flowing when the friction at the wall increased.

- At low liquid loadings or low water cuts, no plugs could be formed since the plate did not promote agglomeration or jamming of hydrates as anticipated.
- Porosity measurements using density scans were usually not feasible since it was almost impossible to drain any liquids from the hydrate slurry.
- No liquid was recovered for these experiments, indicating that most of the water remains trapped in the hydrate phase.
- Permeability measurements were somewhat difficult for several reasons: 1) the permeability calculated is average permeability because the pressure drop is measured across the entire plug. However, the permeability along the plug was variable; 2) almost half of the hydrate formation tests formed a hydrate plug which caused almost no pressure drop built across the hydrate deposit; 3) for the tests which bridged, some of them had gas channels through the hydrate plug which caused pressure drops that were too small to calculate permeability representitive of hydrate plugs; 4) since plugs did not always form at the desired location, it is difficult to estimate the length of the plug formed.

4.1.2 Low Spot Tests

Reproducable plugs of a known length were made under the gamma scan by using a low spot configuration. The main uncertainty in the permeability measurements of the low spot tests were due to gas channels. Liquids were easy to drain in this configuration resulting in porosity measurements of the hydrate deposited. Flow characteristics were investigated as well to study hydrate formation as a function of gas injection. The following conclusions and observations were made.

- The permeability of the plugs formed varied from 2 D to 15 D when measured, but these permeabilities were found to continually decrease as water saturated gas continued to flow through them.
    - It is hypothesized that these plugs would have become impermeable to gas if the gas flow was continued for a longer duration.
- The plugs were formed in a reproducible manner. The procedure produced a reproducible plug.
- Porosity for plugs generated in the low spot configuration are repeatable and ranged from 0.70 to 0.86.
- Hydrate formation time depends on operating parameters such as salinity and sub-cooling temperature. For the same operating parameters, the larger sub-cooling temperatures formed hydrates faster and larger salinity formed hydrates slower.
- Flow characteristic curves show lower sub-cooling temperature gives comparatively small driving force to form hydrate in the same. Also, this result gives a prediction of hydrate onset as a function of gas injection volume with low gas injection rate or low gas leaking rate.

4.2 Hydrate Dissociation Conclusions

The conclusions from the hydrate dissociaton study were also summarized into two sets of experiments; pumping and low spot respectively.

4.2.1 Pumping Tests

- *CSM-Plug* model comparisons to experimental data were better when the two-sided depressurization model was used.
- The driving force for the pumping dissociation tests was so large that once the temperature was increased the hydrate plug collapsed, causing the end of collection of useful data.

4.2.2 Low Spot Tests

After significant experimentation, a reproduceble dissociation method was established for the low spot experiments. An inclination angle of +2 degree was needed to allow the water to drain and yet prevent the plug from collapsing when first starting to dissociate. Density traces are taken every 10 to 15 minutes to get the mass change. After a step in temperature (heating) or pressure (depressurization), another step is not taken until integration of the gamma scan mass stabilizes. Water is drained when observed at the lower view port to prevent water accumulation under the density scan. Based on this approach, the following observations/conclusions were drawn:

- When heating was used to dissociate hydrate plugs, the plugs dissociated uniformly as the model predicts.
- The depressurization tests did not dissociate uniformly as expected, which might be caused by plug collapse, water accumulation, ice formation or other unknown reasons.
- Inhibitors dissociate the plug where they are in contact.
- Modeling with variable temperature and pressure inputs yields a better match between simulation results and experimental data than modeling without variable

inputs. *CSM-Plug*'s two-sided depressurization model worked fine for our experimental data. However, the *TU* model yielded better simulation results compared to *CSM-Plug* two-sided depressurization model because it accounted for temperature and pressure change during dissociation**.**

4.3 Future Work

The following future work based on the current hydrate characterization and dissociation study should be conducted:

4.3.1 Hydrate Characterization Studies

More hydrate formation experiments should be conducted to verify the hypothesis for impermeable hydrate plug during longer duration of gas injection.

Based on the failure of the restrictor plate to cause hydrates to form under the scanning densitometer, it is obvious that the understanding of hydrate formation is lacking. Further study of hydrate formation, perhaps with a model hydrate former under atmospheric conditions, should be done.

4.3.2 Hydrate Dissociation Studies

More depressurization dissociation tests should be conducted to verify the depressurization model.

Hydrate plugs with different permeabilities should be dissociated with extended MEG and methanol experiments using large volumes of inhibitor and increased injection rate to get the relationship of dissociation rate to different permeabilities. For these experiments, the concentration of inhibitor in the drained liquids should be measured.

The inhibitor model developed should be able to link to *PVT-Sim* for input data.

Before correlations for hydrate dissociation can be developed, more dissociation experiments should be run under the procedures that were developed in this report.

ACRONYMS

% WT	Percent by Weight
A	Area
AA	Anti-agglomerants
AC	Alternating Current
D	Darcy
DEH	Direct Electrical Heating
KHI	Kinetic Hydrate Inhibitor
LDHI	Low Dosage Hydrate Inhibitors
LL	Liquid Loading
mD	*Millidarcy*
MEG	Monoethylene Glycol
MeOH	Methanol
NG	Natural Gas
P	Pressure
RPM	Revolutions per Minute
STP	*Standard Conditions for Temperature and Pressure*
T	Temperature
TEG	Triethylene Glycol
WC	Water Cut

SYMBOLS

C_p	Heat Capacity
C_v	Flow Coefficient
$f(l)$	Flow Characteristic
g_s	Specific Gravity
ho	Outside Heat Transfer Coefficient
k	Permeability
Q	Heat Loss
q	Flow Rate
v	Velocity
φ	Porosity
μ	Viscosity
ρ	Density

REFERENCES

1. Austvik, T. "Hydrate Formation and Behavior in Pipes, in Division of Thermodynamics University of Trondheim," The Norwegian Institute of Technology, Trondheim, Norway, 1992, pp. 280.
2. Bear, J. "Dynamics of Fluids in Porous Media, " Dover, ISBN 0-486-65675-6, 1972
3. Berge, L.I., Gjertsen, L.H.and Lysne, D., "Measured Permeability and Porosity of R11(CCl_3F) Hydrate Plugs, " Chemical Engineering Science, Vol.53, No.9, pp.1631-1638, 1998
4. Bjørnstad, B., "Direct Heating Avoids Flowline Fouling, " Hart Energy Publishing, LP**,** Houston, Texas, USA, January, 2004
5. Bollavaram, P. and Sloan, E.D., "Hydrate Plug Dissociation by Method of Depressurization, " presented at Offshore Technology Conference in Houston, Texas, USA, 5-8 May, 2003
6. Boxall, J., Davies, S., Koh, C. and Sloan, D., "Predicting When and Where Hydrate Plugs Form in Oil-Dominated Flowlines, " presented at Offshore Technology Conference held in Houston, Texas, USA, 5-8 May 2008.
7. Buffet, B.A., Zatsepina, "Formation of Gas Hydrate from Dissolved Gas in Natural Porous Media" Marine Geosciences, Vol.164, pp.69-77

8. Dale, E., Thomas, F., and Duncan, A., "Process Dynamics and Control," John Wiley & Sons, Inc, 1989.
9. Davie, M.K. and Buffett, B.A, "A Numerical Model for the Formation of Gas Hydrate below the Sea Floor, " Journal Geophys Res-Solid Earth, Vol.106, pp.497-514, 2001
10. Davies, S.R., Ivanic, J. and Sloan, E.D., "Predictions of Hydrate Plug Dissociation with Electrical Heating, " Center for Research on Hydrates & Other Solids, Colorado School of Mines, USA, 2006
11. Davies, S.R., Selim, M.S. and Sloan, E.D., "Hydrate Plug Dissociation," AIChE J. Vol.**52**, pp. 4016–4027, 2006
12. Dellecase, E., Flow Assurance Course, University of Tulsa, Spring 2006.
13. Domingues, R.S., "Hydrates Formation Rates in Loop Experiments" , August, 2009
14. Dullien, F.A.L., "Porous Media Fluid Transport and Pore Structure", Academic Press, New York, USA, 1979
15. Duplat, S., "Investigation of Hydrate Formation and Plugging Tendencies of Inhibited and Non-Inhibited Systems," MSc Thesis, University of Tulsa, OK, USA, 2005.
16. Edwards, M., "First Low Dosage Hydrate Inhibitor Is Field Proven in Deepwater", Pipeline and Gas Journal, 1999, Vol. 226, pp.44.
17. Estanga, D., "Plugging Tendencies of Hydrate Forming Systems During Restart Operations," Master Thesis, University of Tulsa, OK, USA, 2007

18. Frostman, L.M. and Przybylinski, J.L., "Successful Applications of Anti-agglomerant Hydrate Inhibitors, " SPE International Symposium on Oilfield Chemistry, Houston, Texas, 13-16 February 2001
19. Gruehagen, H. and Lim, D. FMC Technologies, "Subsea Separation and Boosting—An Overview of Ongoing Projects, " presented at SPE Asia Pacific Oil and Gas Conference and Exhibition held in Jakarta, Indonesia, 4-6 August 2009
20. Hammerschmidt, E.G. "Formation of Gas Hydrates in Natural Gas Transmissions Lines, " Ind. Eng. Chem. Vol.26, pp.851,1934,
21. Hernandez, O.C., "Investigation of Hydrate Slurry Flow in Horizontal Pipelines," PhD Dissertation, University of Tulsa, Tulsa, OK, USA, 2006.
22. Hester, K. C., Huo, Z., Ballard, A.L., Koh, C. A., Miller, K. T. and Sloan, E. D., "Thermal Expansivity for sI and SII Clathrate Hydrates" *J*. Phys. Chem. B, Vol.111, Issue 30, pp. 8830–8835, 2007
23. Hong, D.N., Gruy, F. and Herri, J.M., "Experimental Data and Approximate Estimation for Dissociation Time of Hydrate Plugs, " Chemical Engineering Science, Vol.61, pp. 1846-1853, 2006
24. Katz, D.K., "Prediction of Conditions for Hydrate Formation in Natural Gas," Trans., AIME ,Vol. 160.pp.140-149,1954
25. Kvamme, B., "A New Theory for the Kinetics of Hydrate Formation," Proceedings of the Second International Conference on Natural Gas Hydrates, Toulouse, France, pp.131–146, June 2–6, 1996
26. Kvenvolden, K.A., "Methane Hydrate—A Major Reservoir of Carbon in the Shallow Geosphere, " Chemical Geology ,Vol. 77, pp. 41,1998

27. Long, J.P., "Gas Hydrate Formation Mechanism and Kinetic Inhibitor," Ph.D. Thesis, T-4265, Colorado School of Mines, Golden, CO, USA ,1994

28. Lysne, D. "An Experimental Study of Hydrate Plug Dissociation by Pressure Reduction," D.Ing. thesis, University Trondheim, Norges, Tekniske Hogskole, pp.7-9, 1995

29. Mokogon, Y.F., "Natural Gas Hydrate: The Stat e of Study in the USSR and Perspectives for Its Use" Third Chemical Congress of North America, Toronto, Canada, June 5-10, 1988

30. Moridis, G., Collett, T., Boswell, R., Kurihara, M., Reagan, M., Koh, C. and Sloan, D. "Toward Production from Gas Hydrates: Current Status, Assessment of Resources, and Model-Based Evaluation of Technology and Potential," Unconventional Reservoirs Conference held in Keystone, Colorado, USA, 10-12 Feb 2008.

31. Pedersen, K.H., *PVT-Sim* [Computer software developed by Calsep], Houston, Texas, USA, December, 2008

32. Pickering, P.F., Edmonds, B., Moorwood, R.A.S., Szczepanski, R. and Watson, M.J., "Evaluating New Chemicals and Alternatives for Mitigating Hydrates in Oil & Gas Production, " presented at Oil and Gas Exploration and Production Conference, Aberdeen, Scotland, September, 2005

33. Sloan, E.D., "Clathrate Hydrates of Natural Gases," 2nd Edition, Marcel Dekker Inc., 1998.

34. Sloan, E.D., "Hydrate Engineering," 1st Edition, SPE, Richardson, TX, USA, 2000.

35. Sloan, E.D., "Offshore Engineering Hydrate Handbook," ARCO Exploration and Production Technology Co, Golden, Colorado, USA, January, 1998.

36. Sloan, E.D., Koh, C.A., *CSM-Plug*(version 2.1), [Hydrate Dissociation Program], Center for Hydrate Research, Department of Chemical Engineering, Colorado School of Mines, Golden, Colorado, USA, January 2007

37. Stern L.A., Kirby, S.H. and Durhan, W.B., "Peculiarities of Methane Clathrate Hydrate Formation and Solid-state Deformation, Including Possible Superheating of Water Ice," Science, Vol. 273, Issue 5283, pp.1843-1848,1996

38. Vu, V.K., Fantoft, R., Shaw, C. and Gruehagen, H, "Comparison of Subsea Separation Systems," presented at Offshore Technology Conference, Houston, Texas, USA, and 4-7 May, 2009.

39. Wang, D., Liang, D. and Fan, S., "Formation and Blockage of HCFC-141B Hydrate in Pipeline," presented at Proceedings of the 6th International Conference on Gas Hydrates (ICGH 2008), Vancouver, British Columbia, Canada, July 6-10, 2008.

40. Yousif, M.H. and Dunayesky, V.A., "Hydrate Plug Decomposition: Measurements and Modeling, " presented at SPE Annual Technical Conference & Exhibition held in Dallas, USA, 22-25 October, 1995

APPENDIX A

HYDRATE PLUG POSSIBLE LOCATIONS-PUMPING TESTS

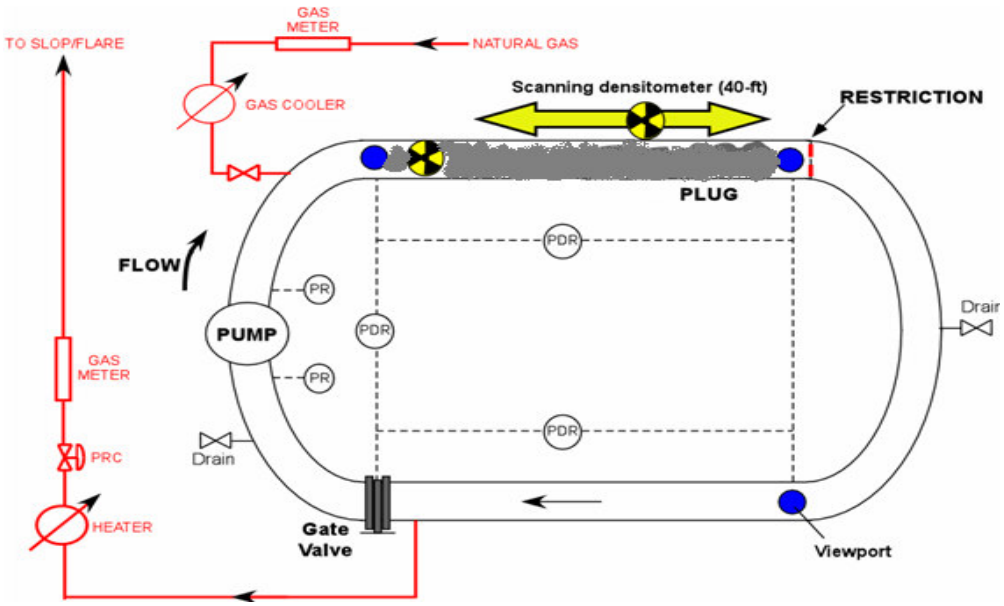

A.1. Impermeable Hydrate Plugs-Bridged

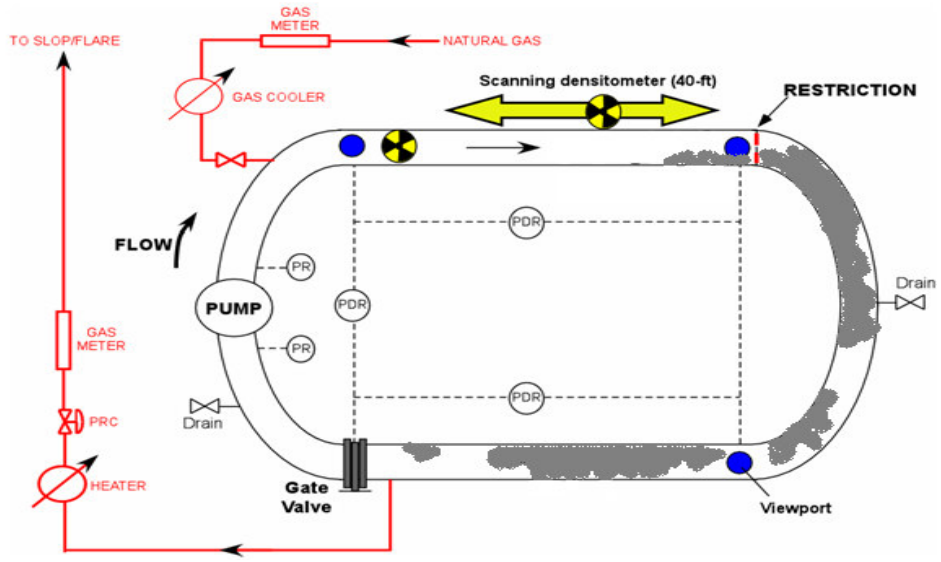

A.2. Partial Hydrate Plugs

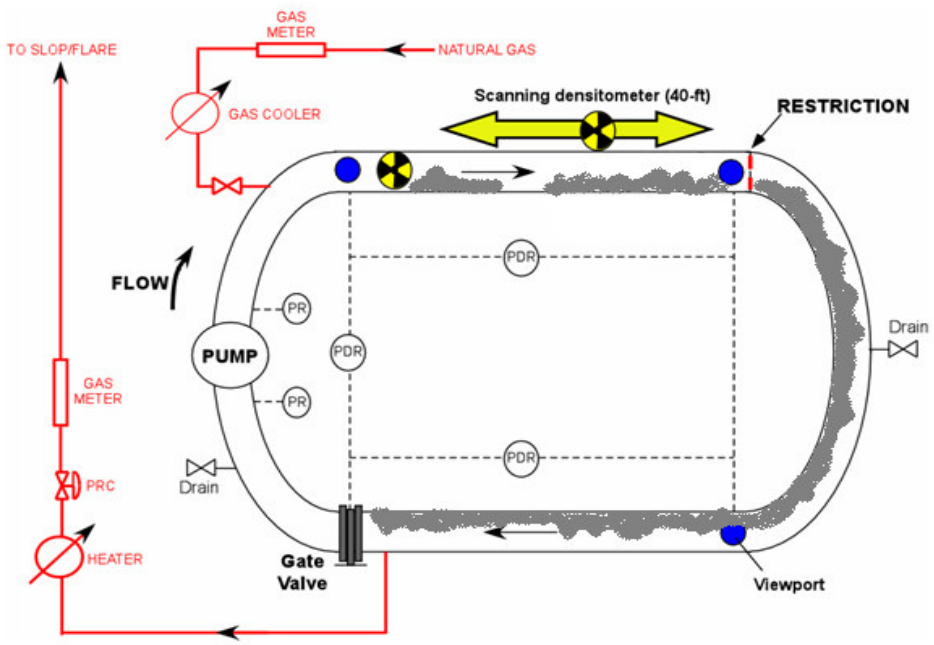

A.3. Deposits with Voids and Channels

APPENDIX B

DENSITY TRACES-PUMPING TESTS

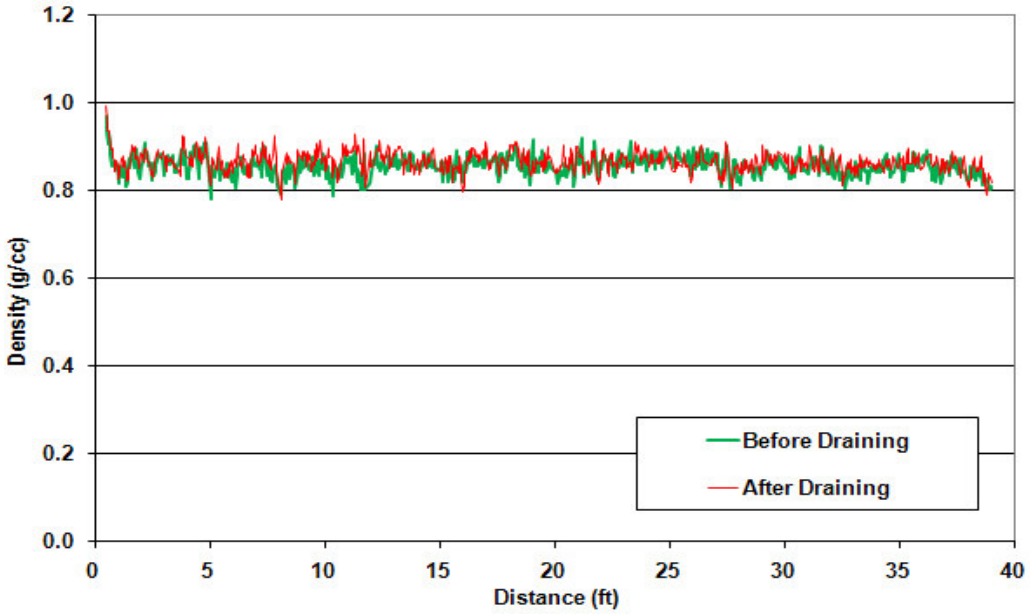

B.1. Impermeable Hydrate Plugs-Bridged—HYD2008-014

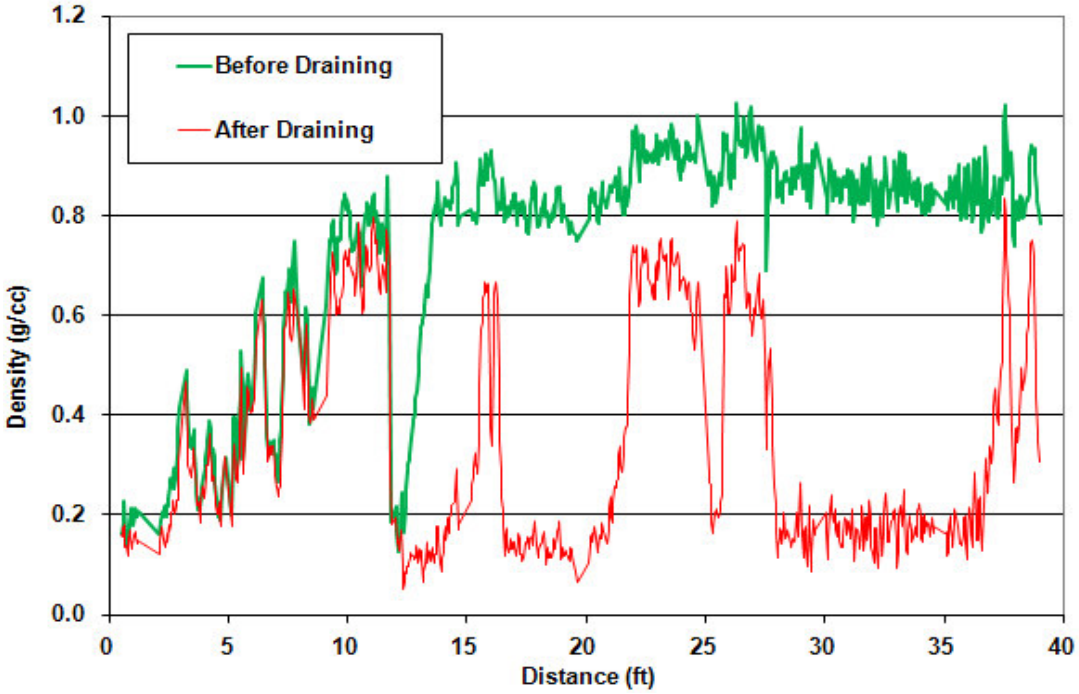

B.2. Partial Hydrate Plugs— HYD2008-025

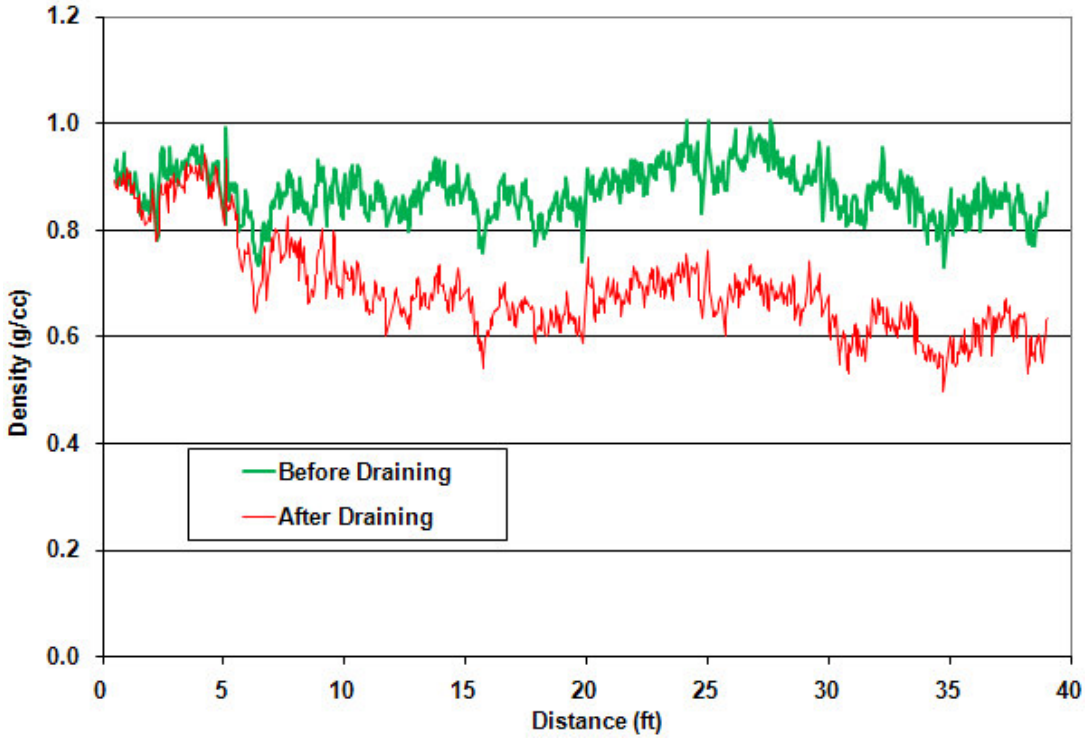

B.3. Deposits with Voids and Channels-Case 1— HYD2008-023

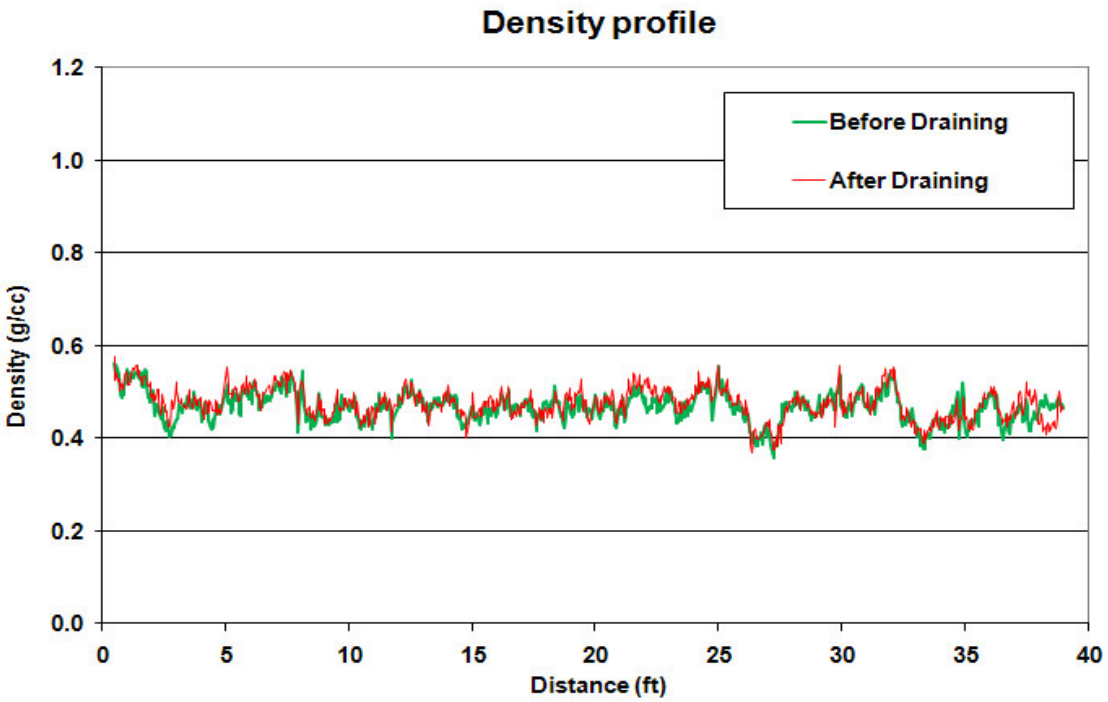

B.4. Deposits with Voids and Channels-Case 2— HYD2008-012

APPENDIX C

PRESSURE DROP & PERMEABILITY MEASUREMENT-PUMPING TESTS

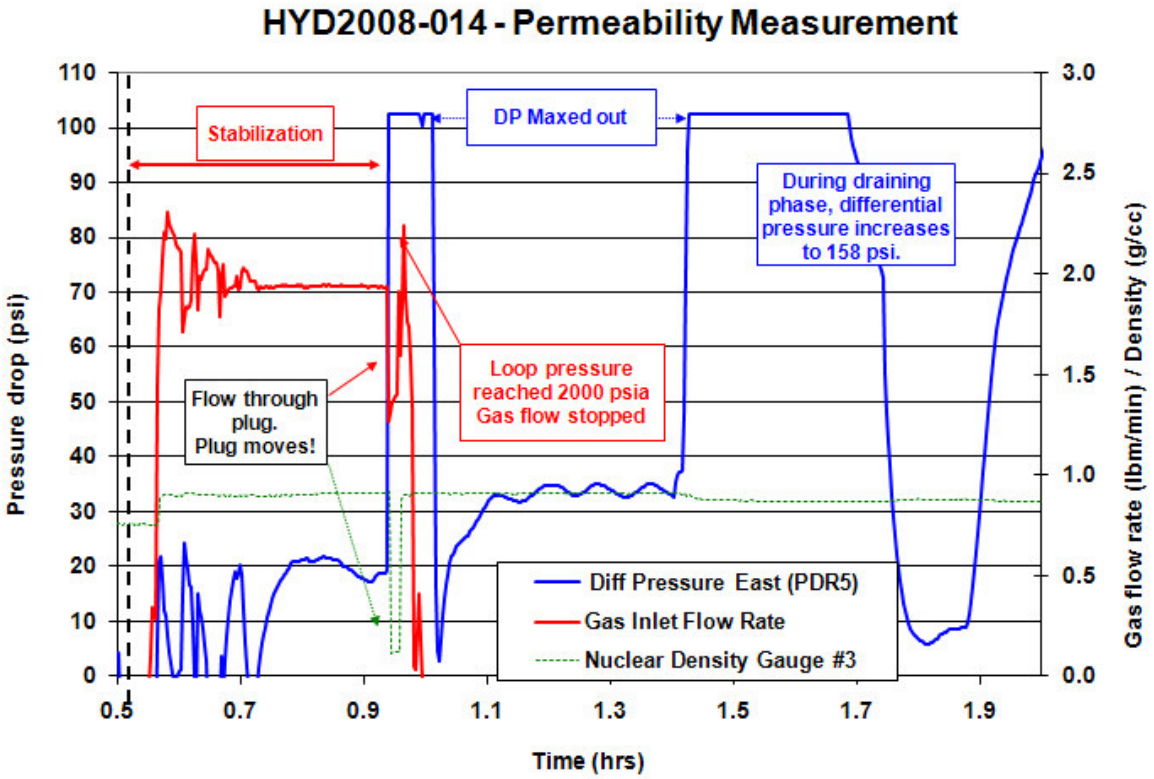

C.1. Pressure & Permeability Measurement of Impermeable Plug under Gamma Scan

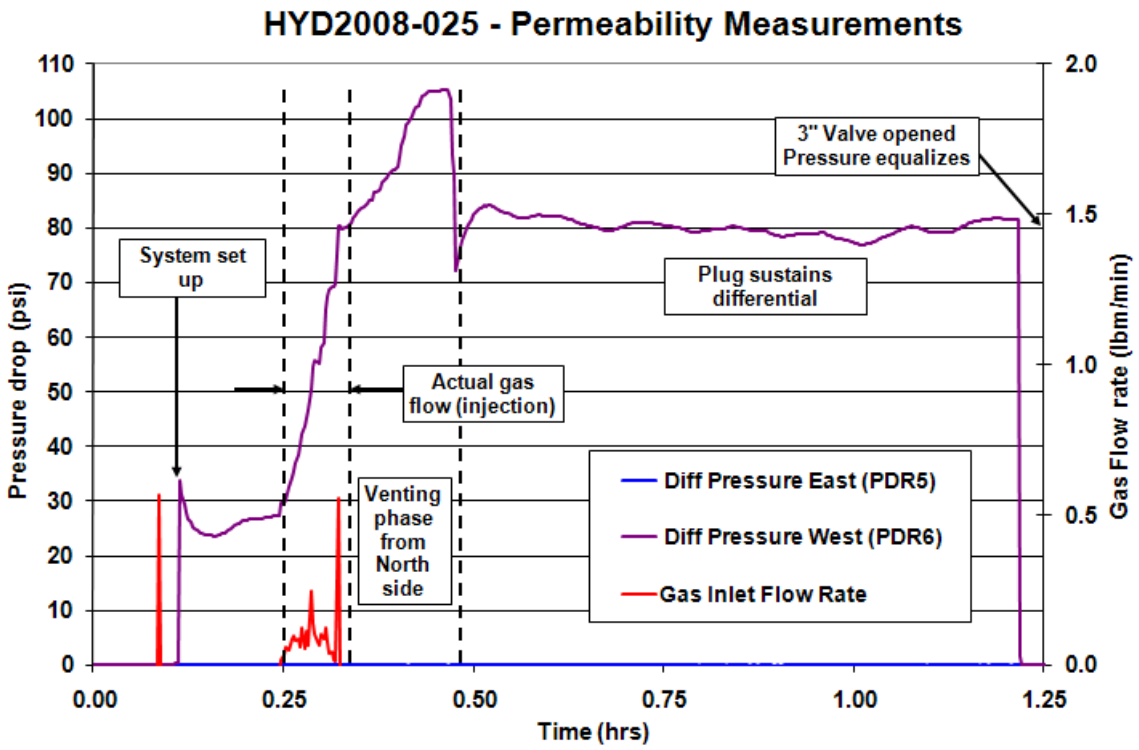

C.2. Huge Permeability Case due to Void Space

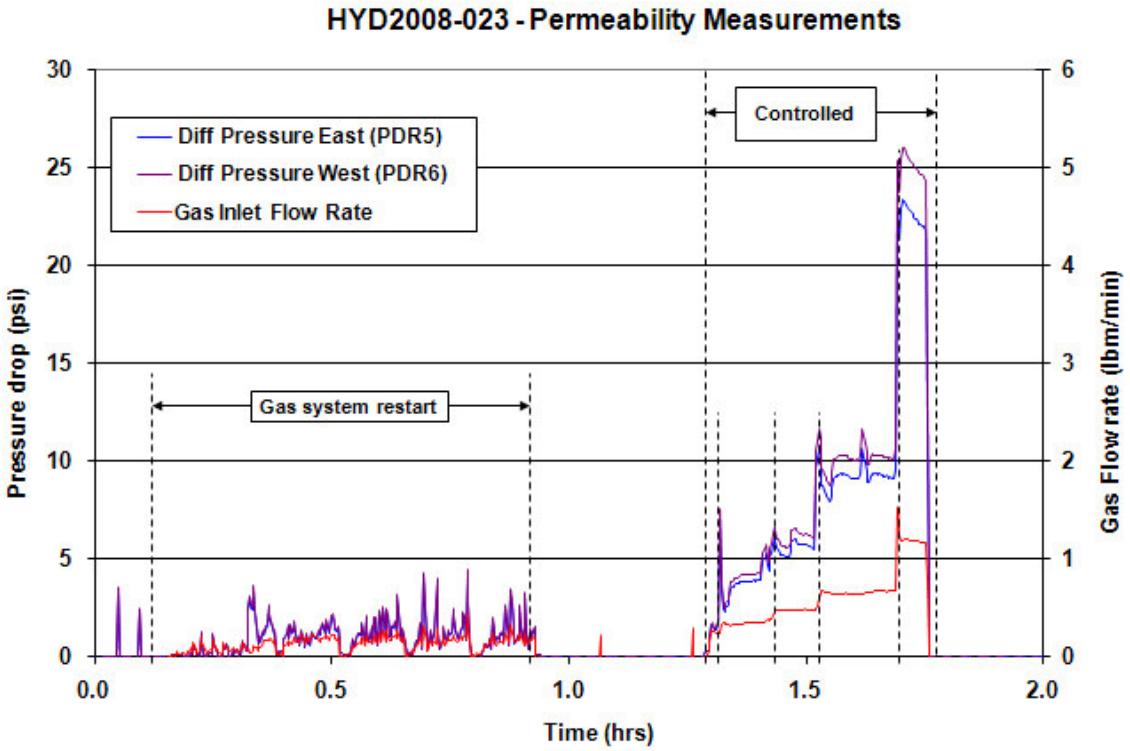

C.3. Uncertain Permeability due to Uncertain Length

APPENDIX D

PERMEABILITY MEASUREMENT-LOW SPOT TESTS

D.1 Permeability Measurement of 2 *lb/min* Gas Injection Rate

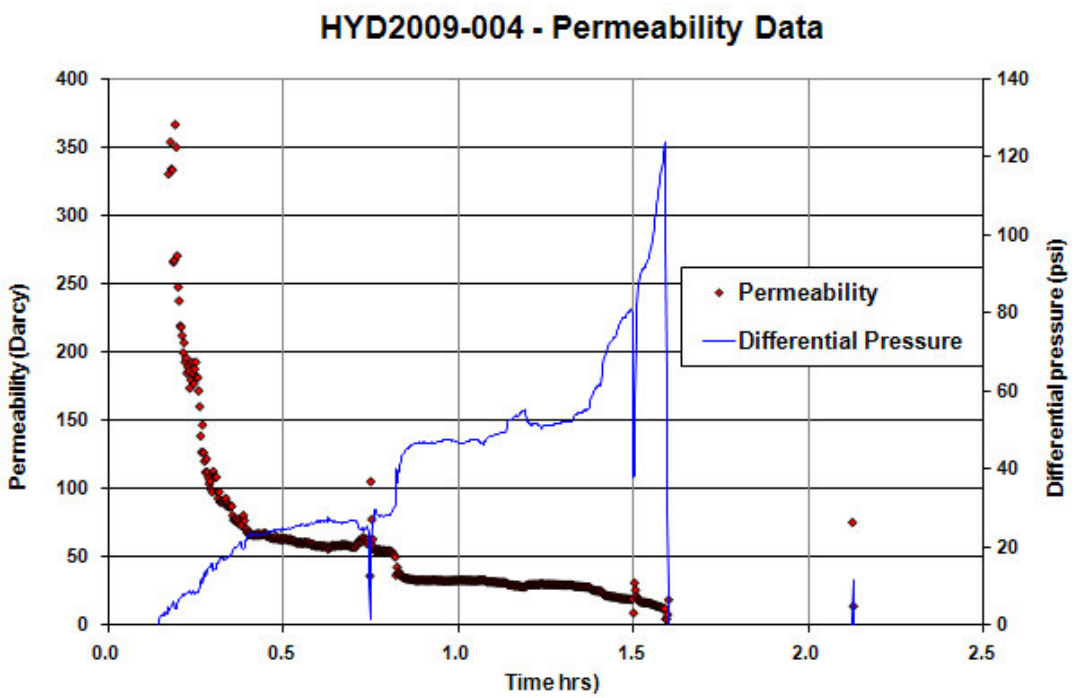

D.1.1. Permeability Measurement--HYD2009-004

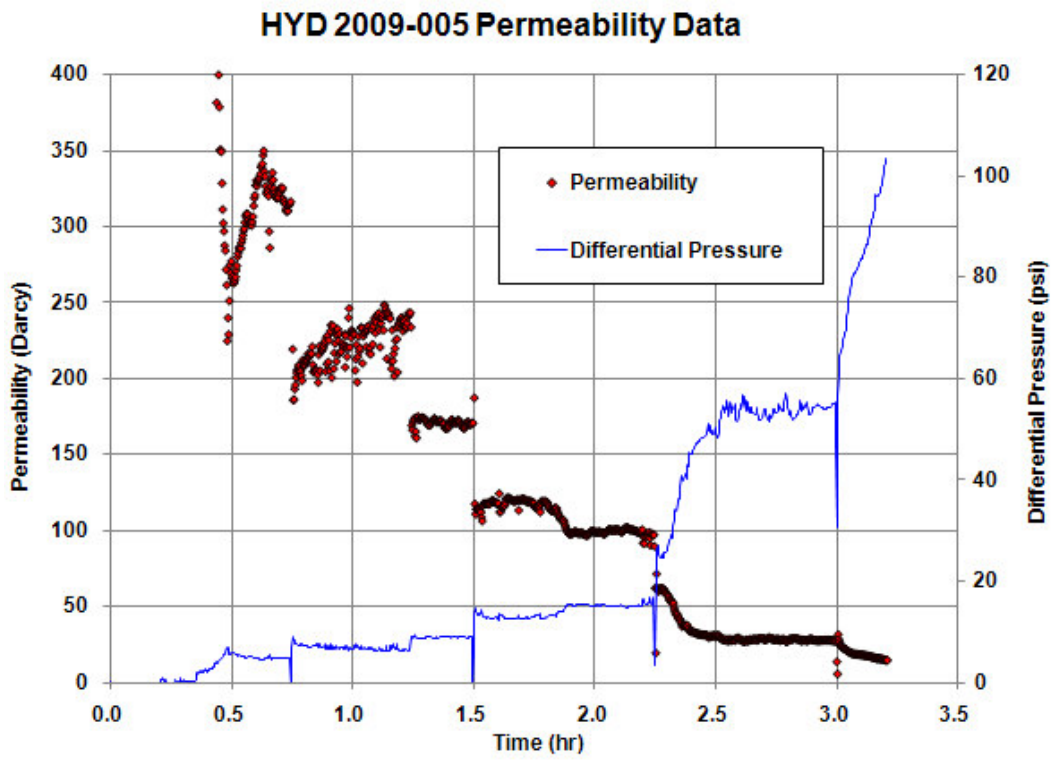

D.1.2. Permeability Measurement—HYD2009-005

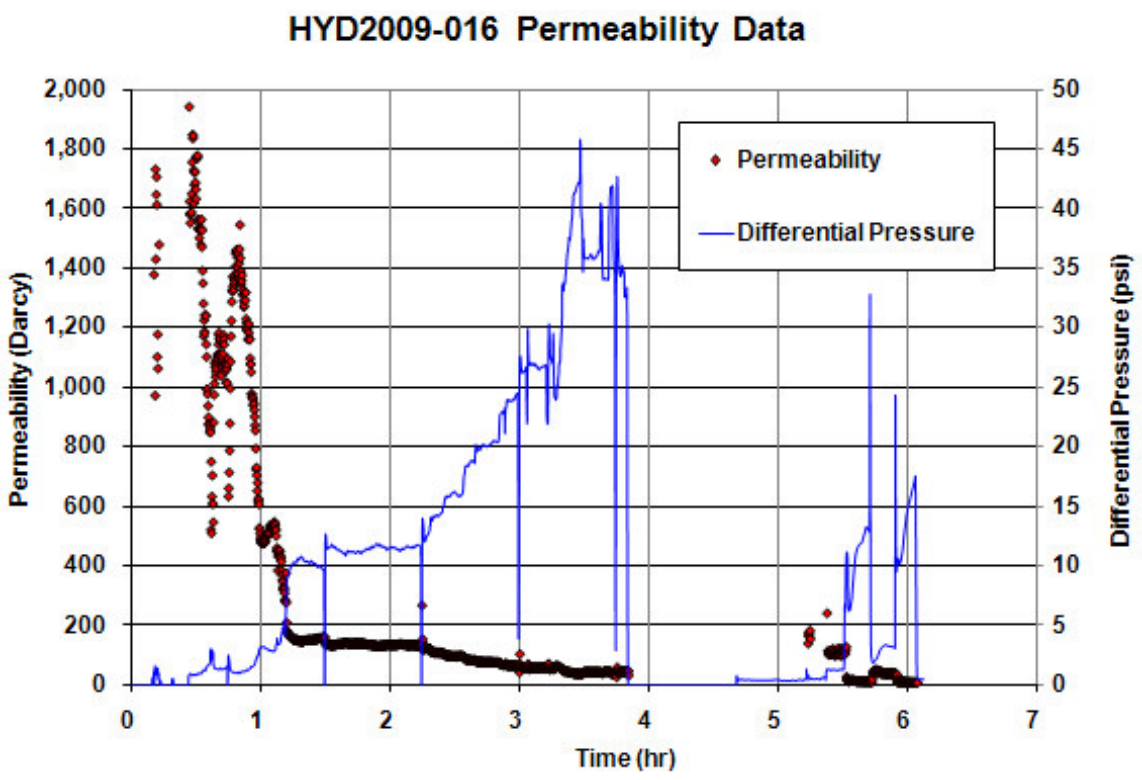

D.1.3. Permeability Measurement—HYD2009-016

D.2 Permeability Measurement of 0.2 *lb/min* Gas Injection Rate

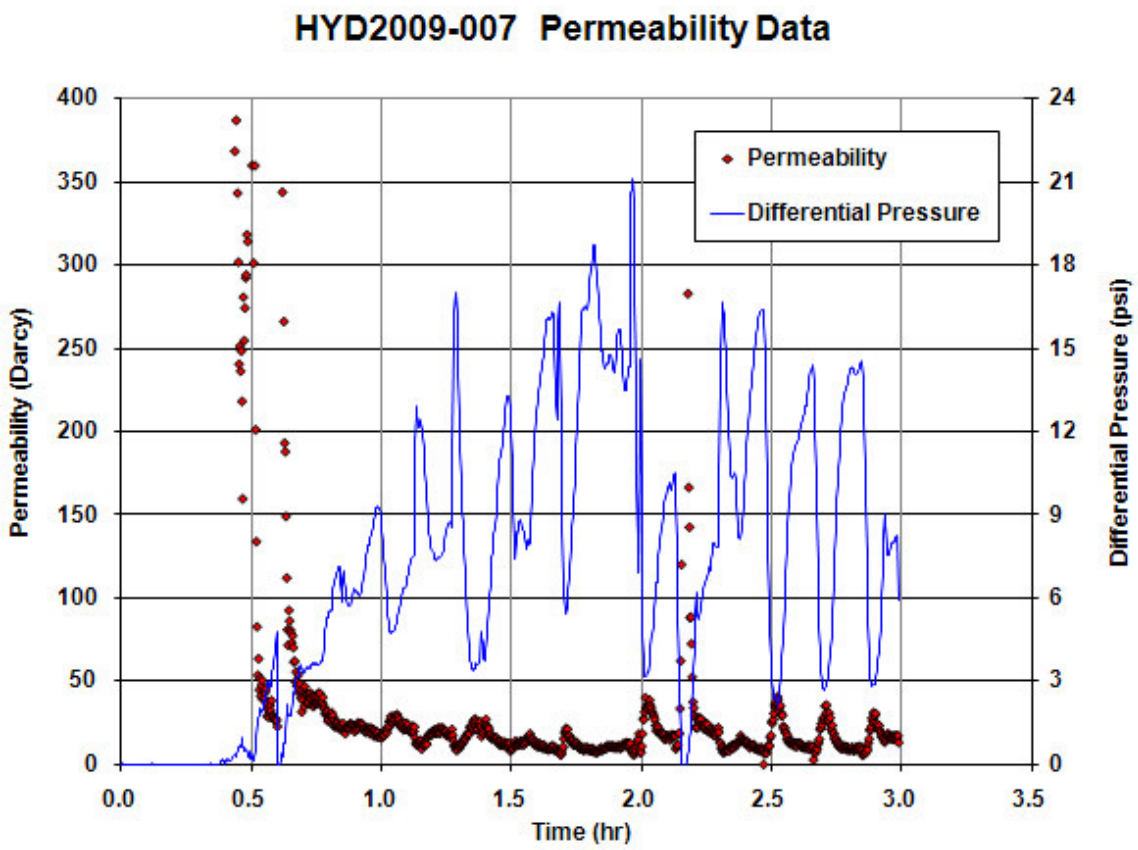

D.2.1. Permeability Measurement—HYD2009-007

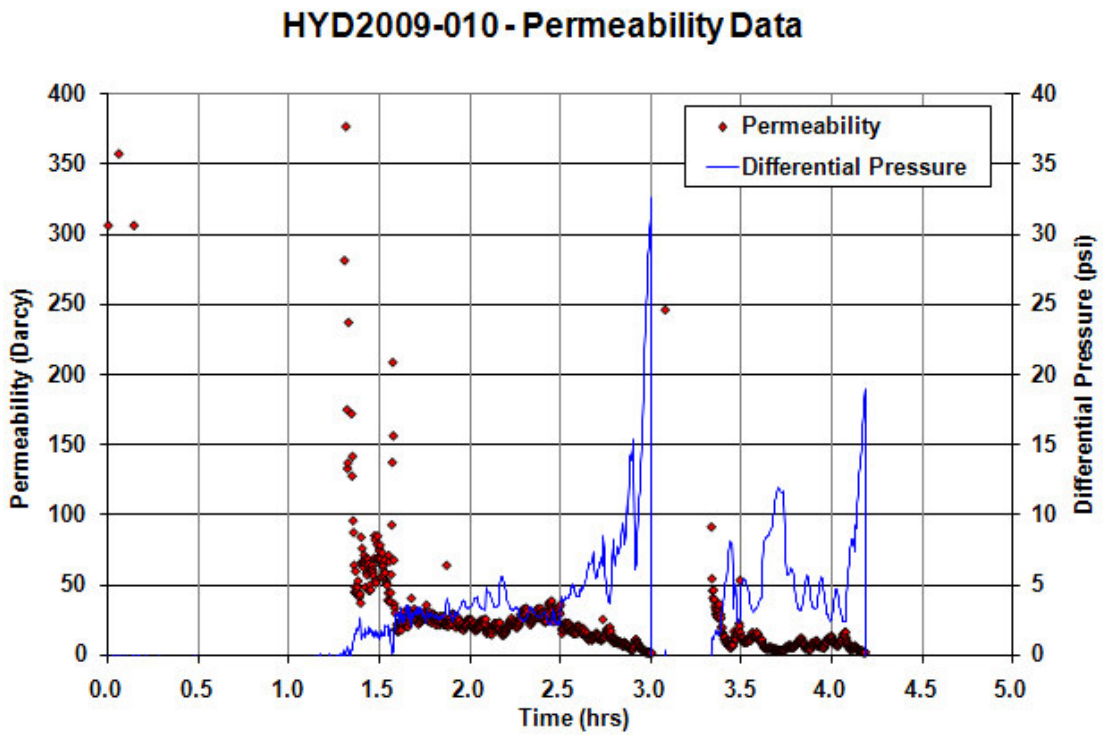

D.2.2. Permeability Measurement—HYD2009-010

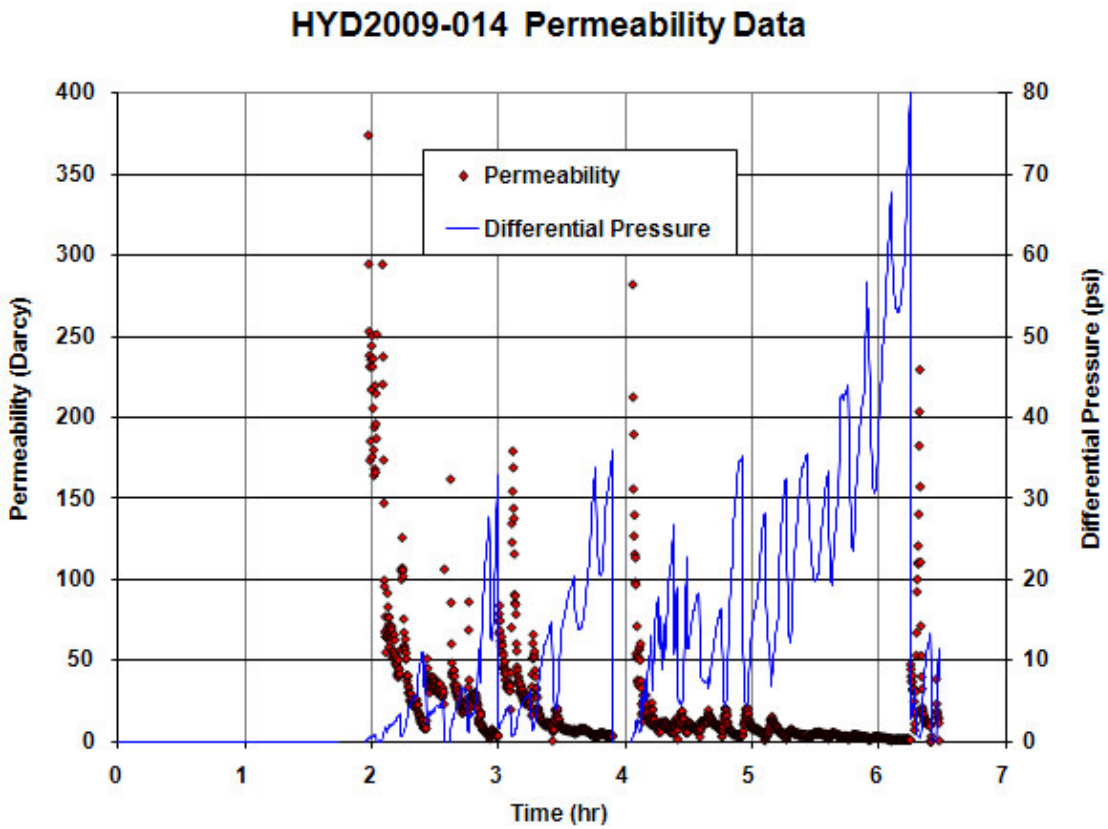

D.2.3. Permeability Measurement—HYD2009-014

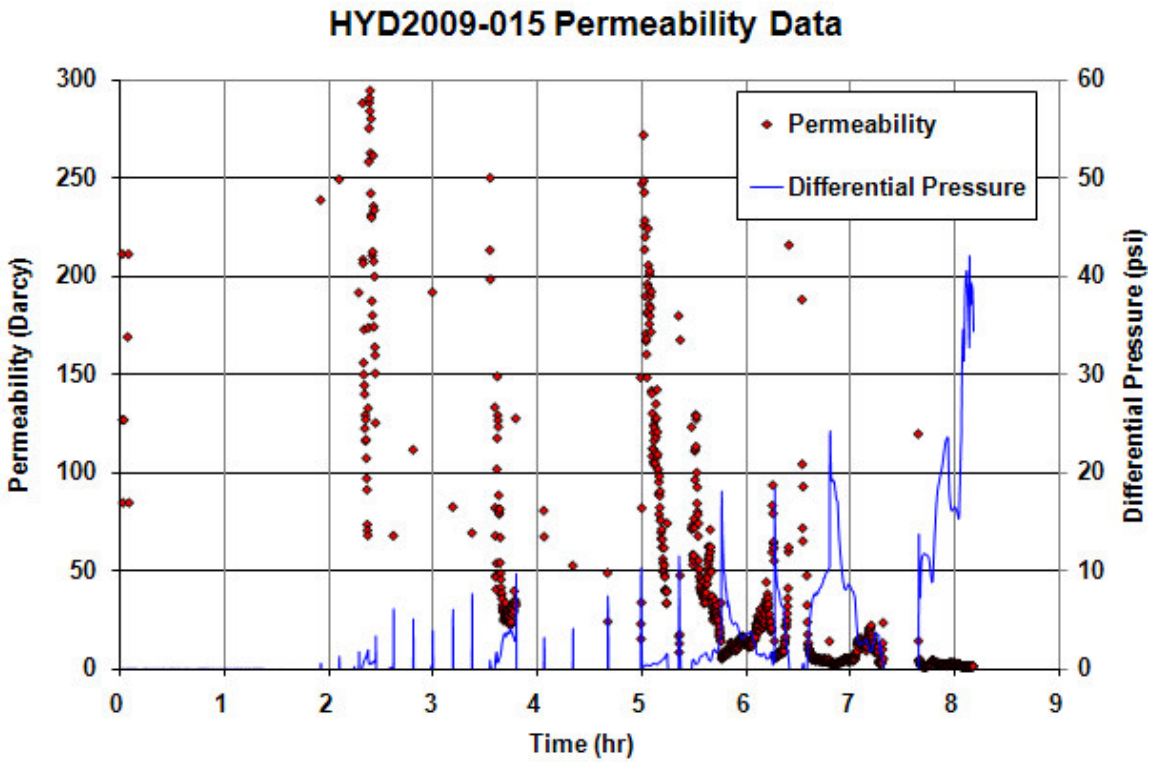

D.2.4. Permeability Measurement—HYD2009-015

APPENDIX E

MODEL SIMULATION BETWEEN *CSM-PLUG* AND *TU* MODEL

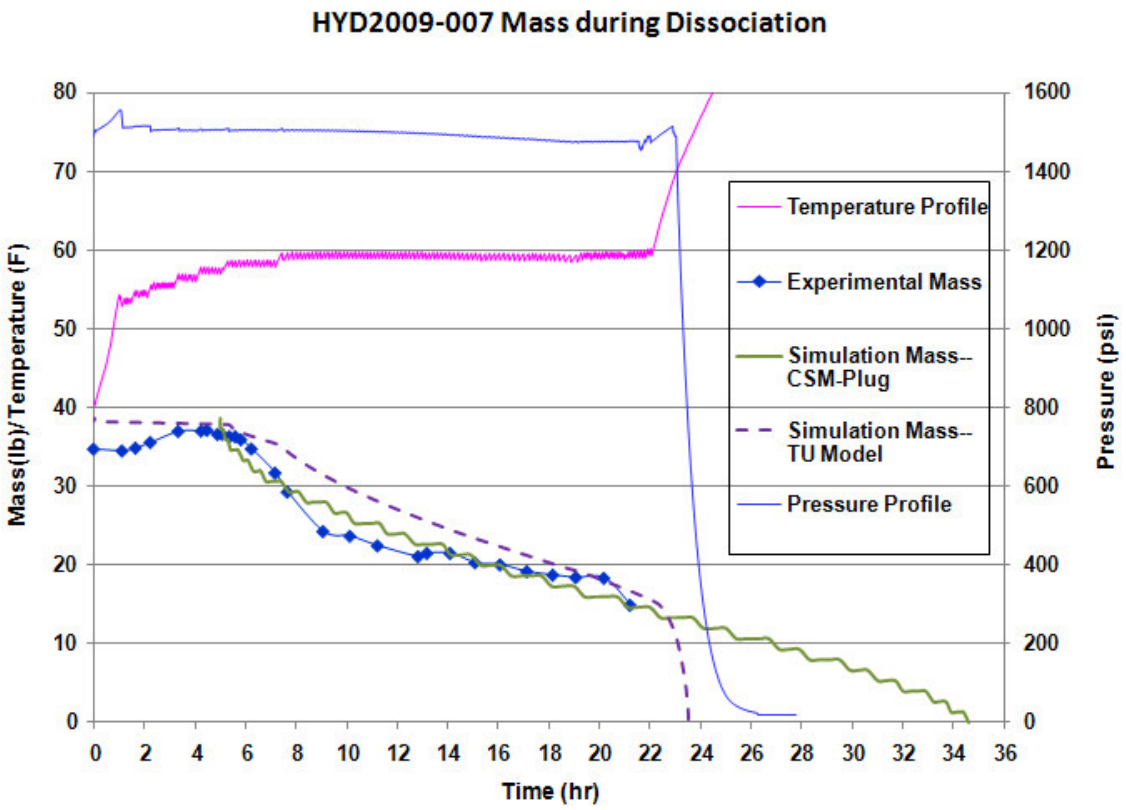

E.1. Model Simulation between *CSM-Plug* and *TU* Model—HYD2009-007

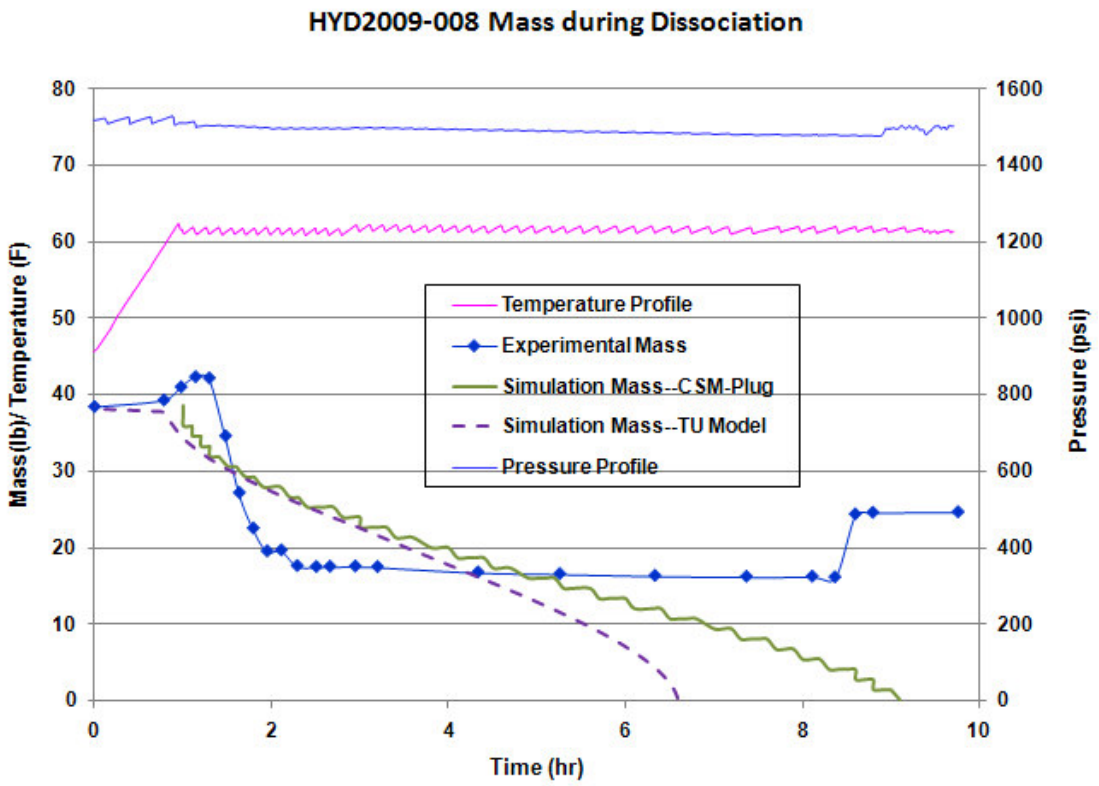

E.2. Model Simulation between *CSM-Plug* and *TU* Model—HYD2009-008

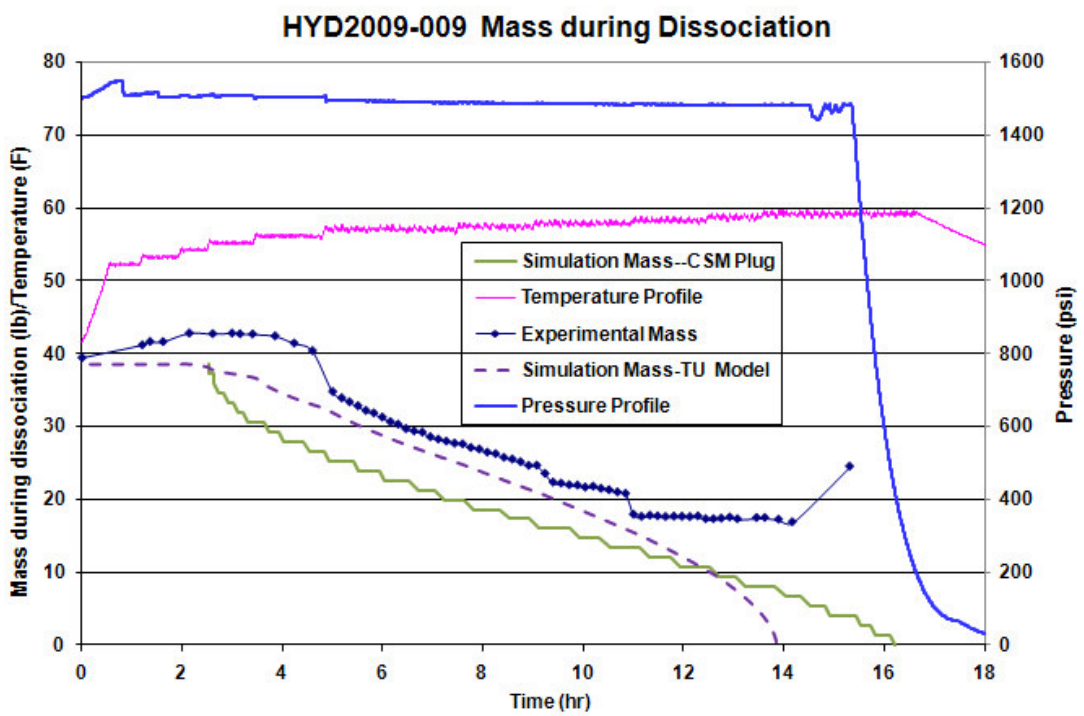

E.3. Model Simulation between *CSM-Plug* and *TU* Model—HYD2009-009

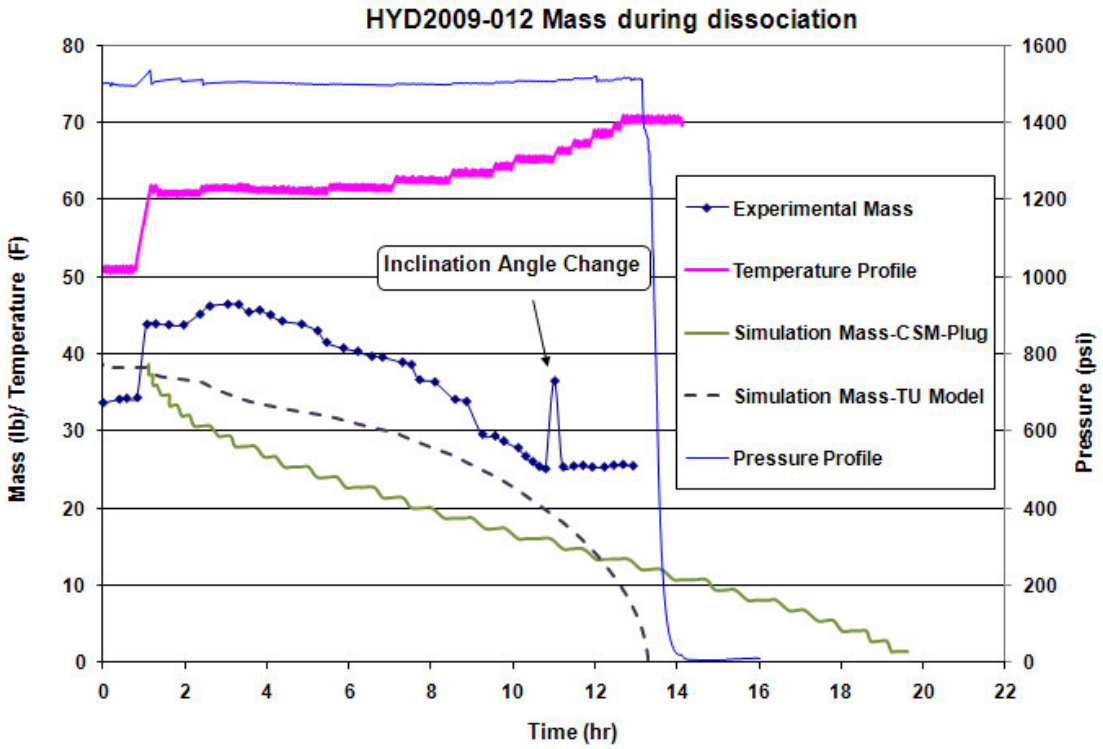

E.4. Model Simulation between *CSM-Plug* and *TU* Model—HYD2009-012

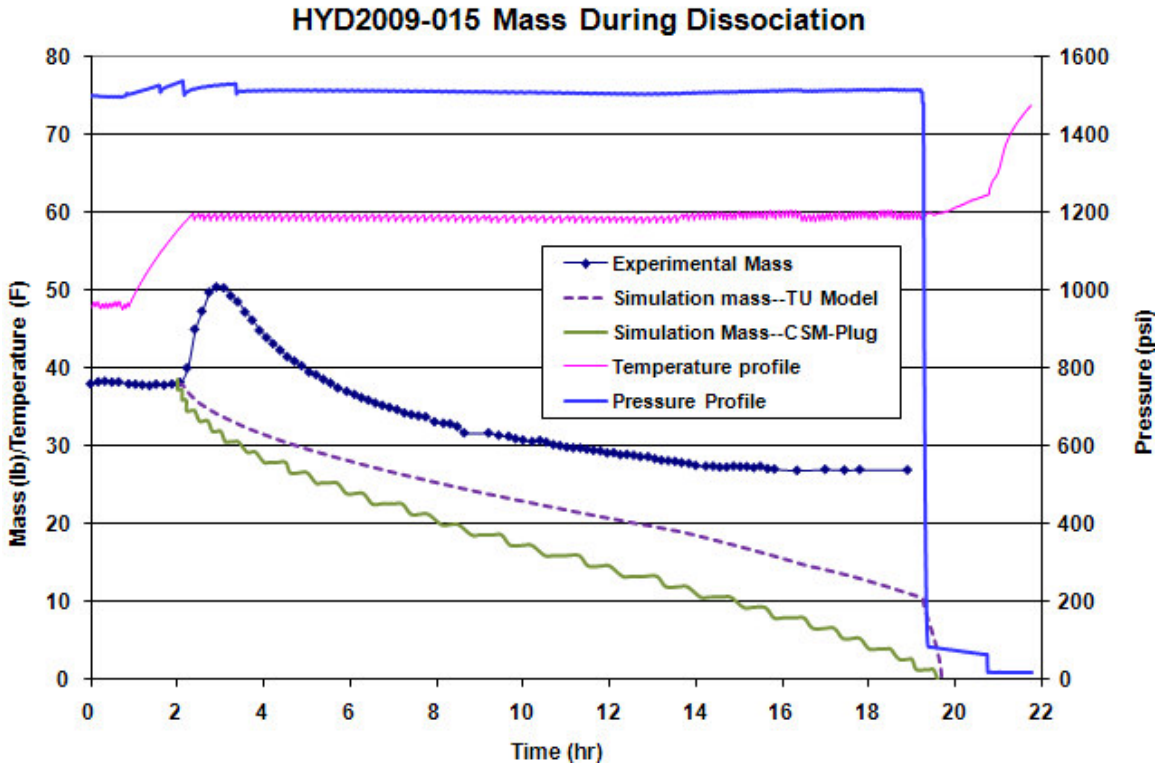

E.5. Model Simulation between *CSM-Plug* and *TU* Model—HYD2009-015

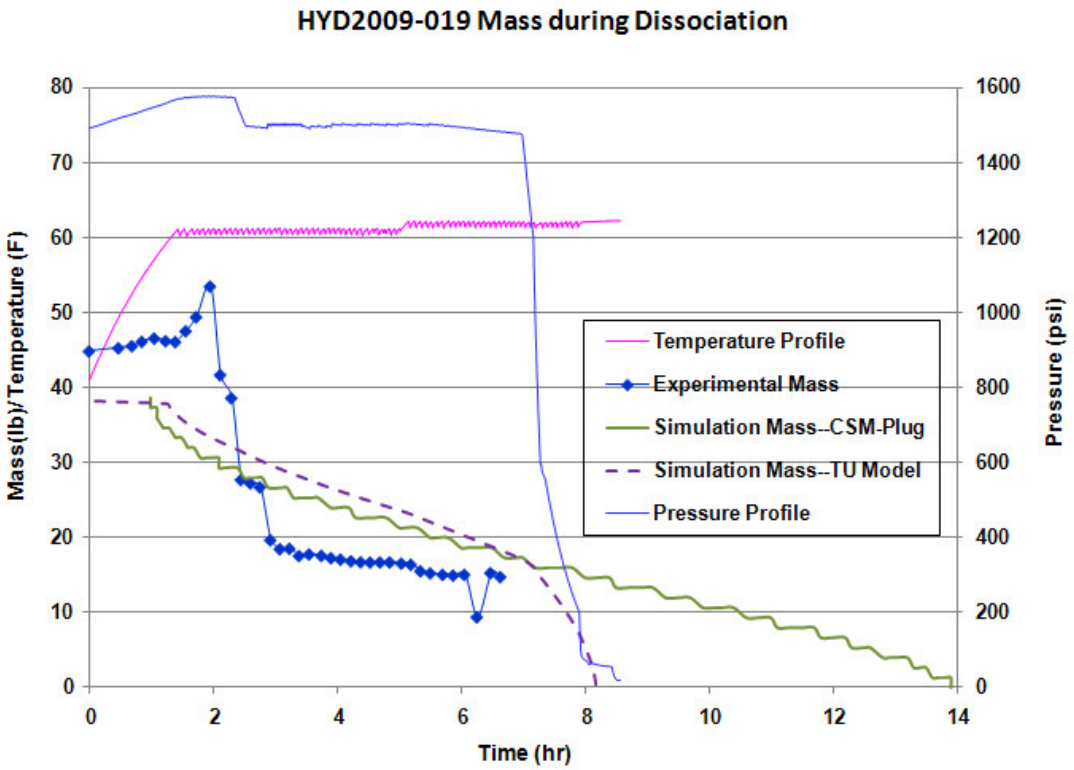

E.6. Model Simulation between *CSM-Plug* and *TU* Model—HYD2009-019

APPENDIX F

TU MEG DISSOCIATION MODEL INSTRUCTIONS

This Excel/VBA program is designed to simulate the dissociation of a methane hydrate plug with monoethylene glycol.

The user may enter data in cells that are light green on the MEG Dissociation tab.

These data are:	Pipe diameter	*inches*
	Initial temperature	*°F*
	Ambient temperature	*°F*
	Porosity	
	Initial MEG weight percent	
	MEG addition rate	*lbm/hr*
	MEG additive weight percent	
	Plug length	*ft*

Properties of water, MEG, and hydrates are hidden in rows 11 - 28.

The entire plug is assumed to be at the initial temperature and 1500 *psi*, with no liquid in the pore spaces. The MEG/water solution is assumed to enter the plug at the initial temperature.

The Init_diss. tab calculates the dissociation of the outer ring of hydrate to the first radial grid point. This step is done automatically by Excel.

For dissociation from the first grid point to the centerline or the end of the plug, whichever comes first, the user must click on the button on the MEG Dissociation page that says "Click here to run the dissociation calculations".

The visual basic code calculates the dissociation and heat transfer as the MEG moves through the plug. The code reports the data back to the MEG Dissociation worksheet every 100 time steps. When the dissociation reaches the pipe centerline, the calculated dissociation time (highlighted in yellow on the MEG Dissociation tab) is finally correct.

Radial heat transfer is calculated first.

$$T_j^{n+1} = T_j^n + \tau\alpha_w \left[\frac{1}{2r} * \frac{-T_{j+1}^n + T_{j-1}^n}{h} + \frac{T_{j+1}^n - 2T_j^n + T_{j-1}^n}{h^2} \right]$$

where

τ = time step

h = radius step in the water; replace α_w with α_H in the hydrate

$T_{99} = T_{98}$ so that there is a zero temperature gradient at the center

$r(j=1) = r_{wall}$

$r(j=99) = 1$ grid point from center

Then the movement of the hydrate/water front is calculated.

$$r_H^{n+1} = r_H^n - \frac{\tau}{h(1-\phi)\rho_H \Delta H_{diss}} \left[k_w \left(T_{j-1}^n - T_j^n \right) - k_H \left(T_j^n - T_{j+1}^n \right) \right]$$

where $T_j^n = T_{diss}$

T_{j-1}^n = lowest water T (just next to hydrate)

T_{j+1}^n = lowest hydrate T (just next to water)

τ = time step

h = radius step

Then the new MEG concentration is calculated, including MEG solution that has moved into the plug. The MEG solution that moves into the plug is mixed with whatever liquids are already in the length of plug in contact with MEG. Water from dissociation in this time step is included.

Then the new MEG concentration is calculated, including MEG solution that has moved into the plug. The MEG solution that moves into the plug is mixed with whatever liquids are already in the length of plug in contact with MEG. Water from dissociation in this time step is included.

After the new MEG concentration is established, the new dissociation temperature is calculated from the following equation, assuming 1500 *psi*.

$$\boxed{T_{dissociati\ on}\left({}^{o}F\right) = -0.616 * \left(weight\%MEG\right) + 61.96}$$

In moving to the next iteration, we assumed that the ring of hydrate dissociated in the previous time step would also be dissociated in the next time step. This means that our calculated dissociation time is an underestimate.

The final dissociation time is calculated once the hydrate/water front moves past the last grid point by extrapolating from the last 3 radius/time data points.

$$\boxed{t_{dissociation} = \frac{r_2 r_3}{(r_2 - r_1)(r_3 - r_1)} t_1 + \frac{r_1 r_3}{(r_1 - r_2)(r_3 - r_2)} t_2 + \frac{r_1 r_2}{(r_1 - r_3)(r_2 - r_3)} t_3}$$

The Dissociation Graph plots the hydrate radius, distance into the plug, MEG concentration, and dissociation temperature as a function of time, but the user will need to adjust the ranges to make the plots correct. There are two different trends for each dependent variable: one from the Init_diss. tab and one from the MEG Dissociation tab.